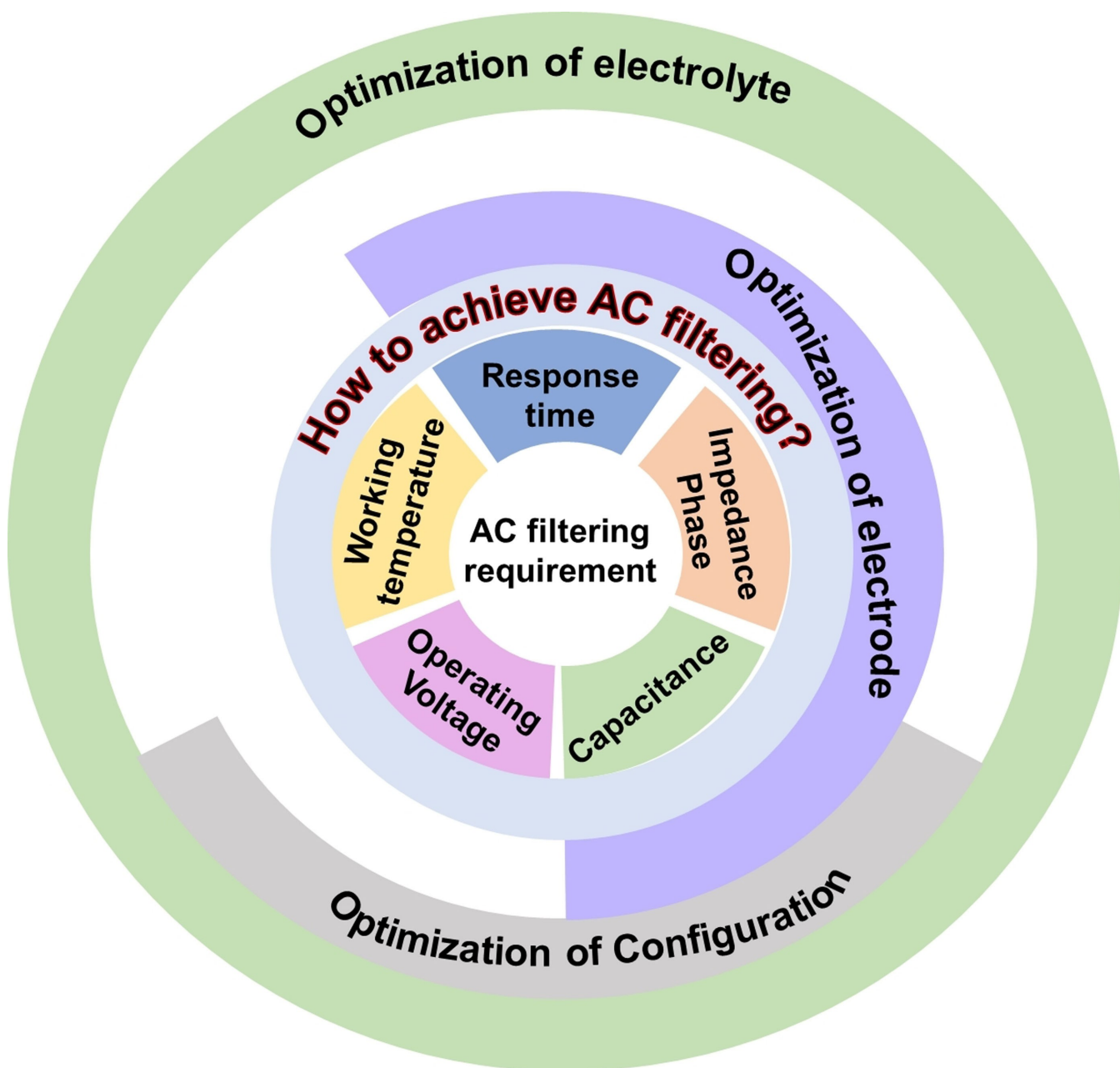


# The Progress and Comprehensive Analysis of Supercapacitors for Alternating Current Line Filtering: A Review

Shuting Zhang,<sup>[a]</sup> Bofan Li,<sup>[a]</sup> Chaojie Cui,<sup>\*[a]</sup> Weizhong Qian,<sup>\*[a]</sup> and Yong Jin<sup>[a]</sup>



To address the potential application of supercapacitors (SCs) in the field of alternating current filtering, this review summarizes the working mechanism toward ultrafast response, the progress of SCs in electrode materials, electrolytes (aqueous, organic electrolyte, and ionic liquids), current collectors, as well as device configuration. The performance of SCs is compared comprehensively with that of the commercial aluminum

electrolyte capacitor (AEC) from the viewpoint of operating temperature, voltage, response time, impedance phase angle, and capacitance. Especially, there exists a big gap between AECs and SCs in terms of the operating temperature and operating voltage. And we give insights into future research focus for high-frequency SCs, in terms of mechanism, structural design, and application management.

## 1. Introduction

Alternating-current (AC) filterers, fundamental components in the circuit of electronics, can attenuate the remaining AC ripple on the direct current (DC) voltage bus to filter out higher harmonics and prevent surges and spikes.<sup>[1]</sup> To date, AC-line filtering with a high-frequency response is accomplished predominantly by aluminum electrolytic capacitors (AECs).<sup>[2]</sup> However, the low volumetric capacitance of AECs occupies a large space in circuits, restricting the miniaturization of portable devices.

Supercapacitors (SCs) exhibit excellent power density<sup>[3]</sup> resulting from the rapidly reversible adsorption and desorption of electrolyte ions on the electrode. SCs can perform a superlong cycle life of up to 1 million cycles, which is very suitable for applications requiring a long duration. Moreover, SCs exhibit a much higher specific capacitance<sup>[4]</sup> than that of AECs<sup>[5]</sup> and multilayer ceramic capacitors (MLCCs).<sup>[6]</sup> As a result, SCs with high energy density are regarded as promising candidates to replace AECs for next-generation high-frequency devices.

During the attempts to use SCs for AC filtering, it is interesting to trace back the development history. In detail, Du's team<sup>[3a]</sup> demonstrated in 2006 that, the SCs with multi-walled carbon nanotubes (MWCNTs) had a significant jump in rate performance and showed great potential in the field of filtering. Subsequently, Miller's team<sup>[2a]</sup> prepared vertically oriented graphene (VOG) as electrodes and the SCs exhibited excellent frequency performance with an impedance phase angle of 82° at 120 Hz in 2010. This was the first study on ultrafast SCs and was completely different from conventional SCs. In the same year, David's team<sup>[7]</sup> achieved an ultrafast response of up to 20 ms with onion-like nanocarbon electrodes in a 3 V TEABF<sub>4</sub>/PC electrolyte. Recently, a structurally integrated 3D carbon tube grid-based SC exhibited an excellent filtering performance.<sup>[8]</sup> Obviously, these results satisfy the AC filtering requirements for the ultrafast frequency response (8 ms) and impedance phase angle (80° at 120 Hz).<sup>[1c,9]</sup> This is quite attractive and promising, as well as their well-known high specific capacitance, which further stimulates the research and development (R&D) of SCs in this relatively new field.<sup>[10]</sup>

[a] S. Zhang, B. Li, Dr. C. Cui, Prof. W. Qian, Prof. Y. Jin  
Department of Chemical Engineering,  
Tsinghua University  
Beijing 100084 (China)  
E-mail: cuicj06@tsinghua.edu.cn  
qianwz@tsinghua.edu.cn

However, AC filtering applications are also complicated systems, and their performance is determined by various factors. To date, a comprehensive analysis of SCs replacing AECs from the structure/property-performance dependent relationship is lacking.

In this review, we summarize the ultrafast response mechanism of SCs and discuss the structure/configuration-AC filtering performance-dependent relationship. As shown in Figure 1, we conclude the five necessary components of AC filtering, including the response time, impedance phase angle (at 120 Hz), capacitance, operating temperature range, and operating voltage. Importantly, perspectives on future research focus of ultrafast response SCs are provided, in terms of mechanism, structural design, and application management. Such application-driven analysis is usually useful for the development of rapidly growing fields, which can maximize the advantages and strive to improve the shortcomings.

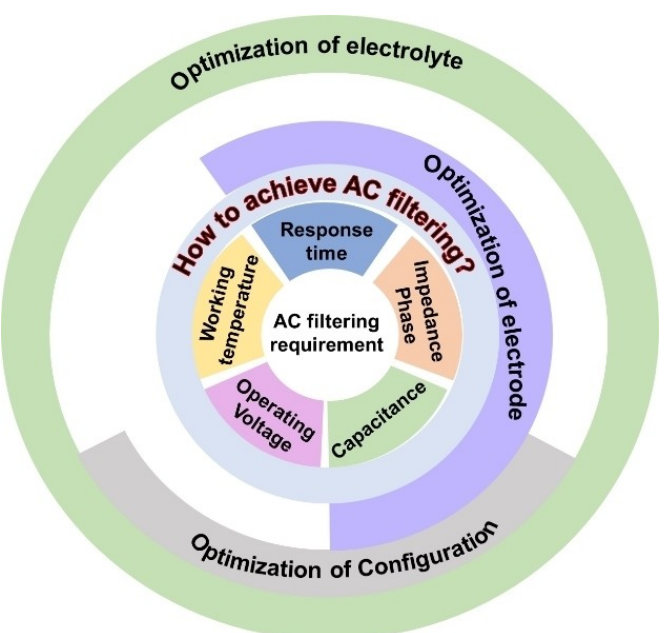


Figure 1. Schematic diagram of five necessary components for AC filtering and the optimization ways for each necessary component.

## 2. Mechanism of the Ultrafast Response for Ultrafast SCs

### 2.1. Charge dynamics based on electrochemical impedance spectroscopy

Since research on the ultrafast frequency response mainly focuses on electric double-layer capacitors (EDLCs), it is of importance to understand the principle of electrical double layer (EDL) energy storage.<sup>[11]</sup> The structure schematic of the SC is shown in Figure 2(a).<sup>[12]</sup> Based on electrostatic adsorption, when the SC is charged, electrolyte ions with opposite charges pass through the complex pores in the electrode and are then adsorbed to the electrode surface forming an EDL (Figure 2b).<sup>[13]</sup> Charge transfer and ion diffusion are closely related to the charge-discharge process of SCs. Essentially, the charge-discharge process of a SC is composed of multiple element rate-determining sub-processes (ERDSPs),<sup>[14]</sup> also known as relaxation sub-processes. They include electron transfer, ion transport in the electrolyte bulk, interface, and pore channels. The time taken for each ERDSP is called the relaxation time.<sup>[14b]</sup> However, charge kinetics are influenced by complex factors including temperature, electrode morphology, interfacial properties, conductivity, and impurities. Because of the different physical mechanisms of each ERDSP, it is difficult to explore charge kinetics clearly by typical methods.

Electrochemical impedance spectroscopy (EIS) can be performed to analyze electrode dynamics by measuring the

variation in impedance with sinusoidal frequency. Combining the equivalent circuit method (ECM), the charge-discharging process of EDLCs can be effectively simplified. To analyze charge dynamics, ECM equivalents the SC interior to a circuit, consisting of a series or parallel connection of the basic elements of resistance ( $R$ ), capacitance ( $C$ ), and inductance ( $L$ ).<sup>[15]</sup>

As shown in Figure 2(c and d), the Nyquist plot of EIS shows a vertical line in an ideal EDLC.<sup>[16]</sup> In comparison, there is an apparent deviation for a practical device, owing to a variety of factors such as internal impedance, electron, and ion impedance.<sup>[18]</sup> In a real EDLC, the equivalent series resistance (ESR) is shown as an intercept with the real axis in the Nyquist plot. The ESR refers to the external resistance generated during assembly and the electrolyte resistance. Moreover, the charge transfer from the electrolyte into the electrode will be hindered at the interface, and is shown as a semicircle in the high-frequency region of the Nyquist plot. The diameter of the semicircle corresponds to the charge transfer impedance ( $R_{ct}$ ). The small  $R_{ct}$  represents the excellent ohmic coupling between the electrode material and the current collector, facilitating rapid charge transfer. In addition, ion diffusion displays a 45° inclined line in the middle-frequency region of the Nyquist plot, which is a typical porous electrode behavior and is defined as Warburg impedance. In the low-frequency region, however, the Nyquist plot often exhibits a near-vertical straight line, which represents an ideal capacitance.<sup>[19]</sup> For a SC, the rate-determining step in the low-frequency region (<100 Hz) is ion migration. As a comparison, the rate-determining step for



Shuting Zhang is a doctoral student at Tsinghua University. She received her bachelor's degree from Dalian University of Technology, Dalian, in 2018. Her research interests focus on the controllable preparation of carbon-based materials and their applications in energy storage (i.e., supercapacitors and aluminum electrolytic capacitors).



Bofan Li is a doctoral student at Tsinghua University. She received her bachelor's degree from the China University of Petroleum, Beijing, in 2019. Her research interests focus on the controllable preparation of carbon materials and their applications in energy storage (i.e., supercapacitors and lithium batteries).



Chaojie Cui entered Tsinghua University in 2006 and received her bachelor's, Master's, and doctor's degrees in 2010, 2012, and 2015, respectively. Since 2018, she worked at Tsinghua University as an assistant researcher. Her research interests cover carbon materials and their applications in energy storage and environmental protection.



Weizhong Qian received doctor's degree at Tsinghua University in 2002. He worked at Tsinghua University as an assistant professor since 2002 and an associate Professor of Chemical Engineering since 2005. His research has been focused on the development of efficient methods to prepare CNTs with high quality on large scale, for commercial applications in energy storage.



Yong Jin is a professor at Tsinghua University and an academician at the Chinese Academy of Engineering. His research areas focus on the basic research and structural design of fluidized bed and his research results have already been successfully applied in industrial processes. Moreover, he has made important breakthroughs in ecological chemical engineering and technology, product engineering, submicron, and nano-powder technology research and application.

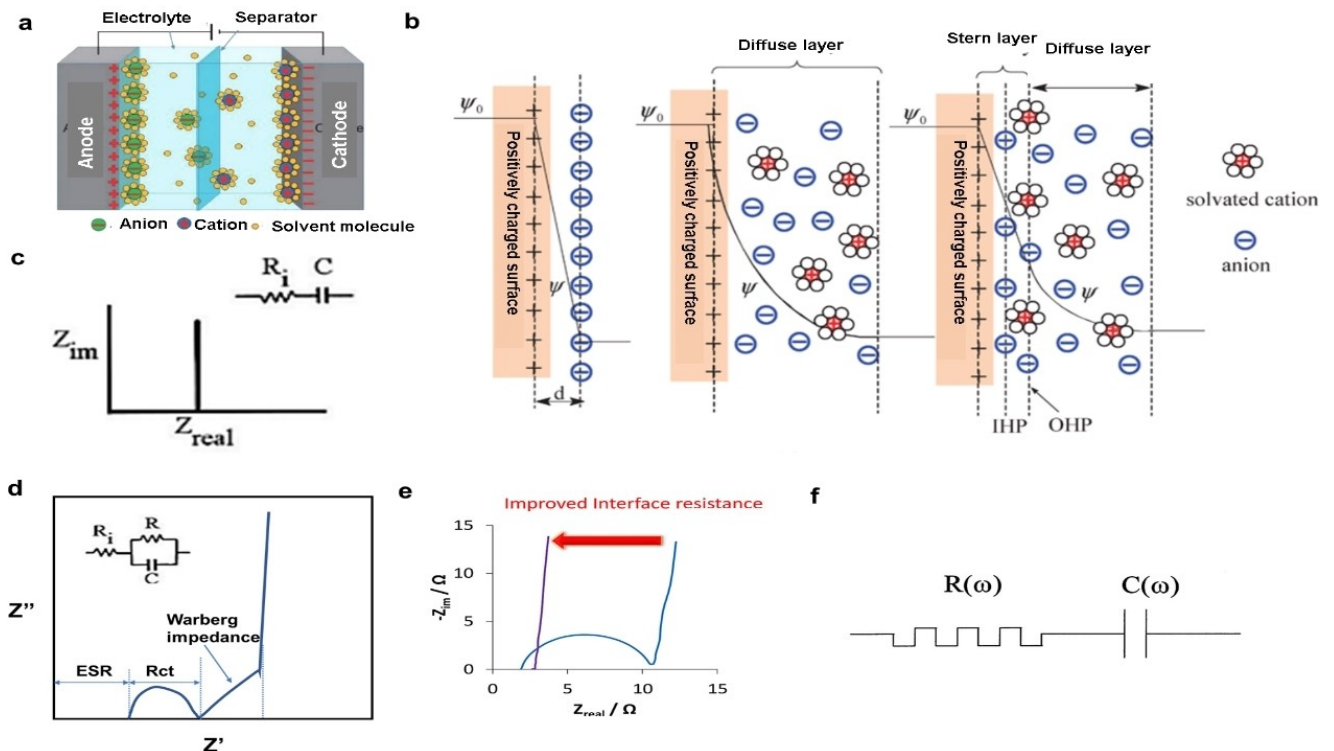


**Figure 2.** a) Schematic representation of an EDLC. Reproduced with permission from Ref. [12]. Copyright (2020) Elsevier. b) Models of the EDLC at a positively charged surface: the Helmholtz model, the Gouy-Chapman model, and the Stern model; Reproduced with permission from Ref. [13b]. Copyright (2009) Royal Society of Chemistry. c) Nyquist plot of an ideal EDLC; Reproduced with permission from Ref. [16]. Copyright (2009) Royal Society of Chemistry. d) Nyquist plot of an actual EDLC; e) Decrease the semicircle of Nyquist plot for ultrafast frequency; Reproduced with permission from Ref. [17]. Copyright (2019) Elsevier. f) The resistor-capacitor series circuit.

the frequency response at high frequency is charge transfer. Obviously, the key to excellent frequency performance should be to ensure both fast electron transfer and ion transport of a SC.<sup>[2a,20]</sup> This is accompanied by the reduction or even absence of semicircles in the Nyquist plot (Figure 2e).<sup>[17]</sup>

Based on the charge dynamics, the electrode material, the current collector, and the interface between the electrode and current collector with different conductivity and morphology affect the electron transfer and electrolyte-ion diffusion. Similarly, electrolytes with different conductivity, viscosity, and ion size have distinct ion diffusion rates, which then affect the electrochemical performance. Therefore, the design of electrode structure is very important in the study of ultrafast SCs.

Notably, the charge dynamics of SCs is still superficial and needs to be studied in depth to improve device performance.

## 2.2. Derivation of the frequency response of SCs

The frequency response performance of SCs is often expressed by the time constant and the impedance phase. The time constant can be expressed in two ways, including the characteristic relaxation time constant ( $\tau_0$ ) and the resistor-capacitor time constant ( $\tau_{RC}$ ). Understanding the derivation of the time constant is helpful for designing SCs with high performance.  $\tau_0$  represents the time required when the device discharge reaches 50% of the maximum efficiency.<sup>[21]</sup> And  $\tau_{RC}$  is

the product of impedance and capacitance at a given frequency, defining the time required for charging to 63.2% of the full potential of the capacitor.<sup>[2a,22]</sup>

First, the  $\tau_0$  can be obtained from the EIS data and is derived as follows.<sup>[1c,2d,10]</sup>

The impedance expression varying with frequency is  $Z(w)$ :

$$Z(w) = 1/(jwC(w)) \quad (1)$$

where  $w$  is the angular frequency,  $C(w)$  is the capacitance at the angular frequency of  $w$ , and  $Z(w)$  is the impedance at the angular frequency of  $w$ .

Since  $Z(w)$  can be expressed as:

$$Z(w) = Z'(w) + jZ''(w) \quad (2)$$

where  $Z'(w)$  is the real part of  $Z(w)$ , and  $Z''(w)$  is the imaginary part of  $Z(w)$ .

The variation of capacitance with frequency can therefore be expressed as  $C(w)$ :

$$C(w) = -\frac{Z''(w) + jZ'(w)}{w|Z(w)|^2} \quad (3)$$

where  $|Z(w)|$  is the absolute value of  $Z(w)$ .

Moreover,  $C(w)$  can also be expressed as:

$$C(w) = C'(w) + jC''(w)$$

$$(4) \quad \tau_{RC} = RC = -Z'/wZ''$$

where  $C'(w)$  is the real part of  $C(w)$ , and  $C''(w)$  is the imaginary part of  $C(w)$ . Here,  $C'(w)$  describes the loss within the SC due to irreversible impedance.

Thus,

$$C''(w) = \frac{Z''(w)}{w|Z(w)|^2} \quad (5)$$

$$C'(w) = -\frac{Z'(w)}{w|Z(w)|^2} \quad (6)$$

Since  $Z(w)$ ,  $Z'(w)$ ,  $Z''(w)$  can be obtained from the EIS test, the Equations  $C'(w)$  and  $C''(w)$  versus frequency can be deduced.

The corresponding frequency at the maximum  $C''(w)$  is called the cutoff frequency ( $f_0$ ), where the real impedance is equal to the imaginary impedance. At this point, the impedance phase is  $45^\circ$ , which is the boundary between the capacitive and resistive behavior of the SC.<sup>[23]</sup> In addition, the reciprocal of the  $f_0$  is called the characteristic relaxation time constant ( $\tau_0$ ).<sup>[21]</sup>

$\tau_{RC}$  needs to be obtained in the RC equivalent circuit model. For porous electrodes of SCs, a transmission line model (TLM) with multiple time constants is usually more accurate.<sup>[24]</sup> However, the single time-constant RC model is a simple but effective approximation method, which is widely employed to describe charge/discharge behavior.<sup>[2d,7,9d,25]</sup> As shown in Figure 2(f), the impedance of the RC circuit can be expressed as:

$$Z(w) = R + \frac{1}{jwC(w)} \quad (7)$$

where  $Z(w)$  is the impedance of the RC circuit at the angular frequency of  $w$ ,  $R$  is equivalent series resistance,  $C(w)$  is the capacitance of capacitor at the angular frequency of  $w$ .

And because of :

$$Z = Z' + jZ'' \quad (8)$$

where  $Z'$  is the real part of  $Z$ , and  $Z''$  is the imaginary part of  $Z$ . Therefore,

$$Z' = R \quad (9)$$

$$C(w) = -1/wZ'' \quad (10)$$

Obviously,

$$C(w) = -1/(2\pi f Z''), \quad (11)$$

where  $Z''$  is the imaginary part of the impedance.

And the expression of the RC time constant is:

Based on the 60 Hz AC frequency in the USA and 50 Hz AC frequency in China, the  $\tau_{RC}$  and the impedance phase angle at 100 Hz/120 Hz are crucial to evaluate the filtering performance.<sup>[10,26]</sup> For AC filtering capacitors, a  $\tau_{RC}$  of 8.3 ms at 120 Hz is generally needed. For an ideal capacitor, the phase is  $90^\circ$  at 120 Hz, while the actual SC behaves like a resistor and the impedance phase is close to  $0^\circ$ . Notably, AECs used in filtering have an impedance phase angle of approximately  $-80^\circ \sim -83^\circ$  at 120 Hz, and a lower phase angle will lead to more heat loss.<sup>[27]</sup>

### 3. Influence of Components on the Performance of the Ultrafast Supercapacitor

Ultrafast SCs should be improved in five aspects: response time, impedance phase angle, capacitance, operating temperature range, and operating voltage. As the key factors for ultrafast performance, electrode materials, current collectors, and electrolytes are mainly discussed in this chapter.

#### 3.1. Electrode materials

The electrode material is the core component of SCs, and its physicochemical properties, such as conductivity and pore structure, play a key role in electrochemical performance.

Because of their high specific surface area and conductivity, porous carbon materials are commonly adopted for traditional SCs.<sup>[12,28]</sup> However, porous carbon materials with high specific surface areas often have complex and tortuous pore channels (Figure 3a),<sup>[29]</sup> which could lengthen the ion transport distance. Especially at the high charge-discharge rate for SCs, electrolyte ions are unable to pass through complex pore channels quickly.<sup>[30]</sup> Moreover, EDLC energy storage in porous carbon is equivalent to a distributed storage charge,<sup>[2a,3b,16,31]</sup> which is unfavorable for an ultrafast response.<sup>[10,32]</sup> Apparently, the electrode material must be conducive to both electron transfer and ion transport to achieve an ultrafast response of SCs. Here, we introduce the research progress on electrodes of ultrafast response SCs.

##### 3.1.1. Carbon-cased materials

To date, 2D carbon materials are regarded as promising electrode materials,<sup>[29]</sup> such as graphene and carbon nanotubes (CNTs).<sup>[30,33]</sup> They are widely adopted for ultrafast response SCs.

VOG is a good choice for high-frequency SC electrodes. It can minimize the porosity effect, thereby providing fast ion transport from the electrolyte bulk to the electrode surface.<sup>[2a,b,25d,34]</sup> Generally, VOG is prepared by radio frequency plasma-enhanced chemical vapor deposition (RF-PECVD). In

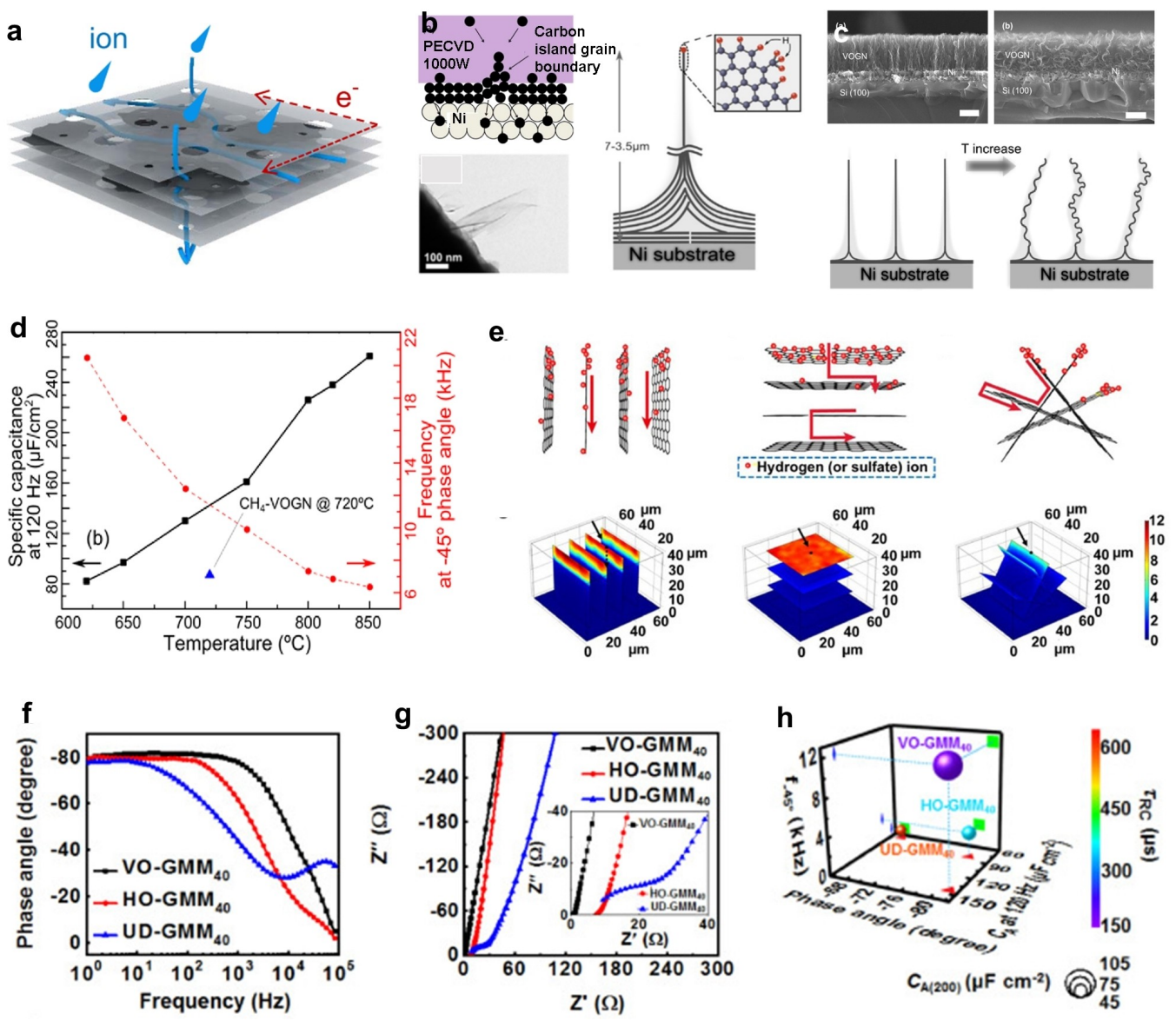


**Figure 3.** a) Schematic illustration of ion diffusion and electron transfer. Reproduced with permission from Ref. [29]. Copyright (2020) American Chemical Society. b) A schematic showing graphite island impingement and upward growth and SEM image of VOG; Reproduced with permission from Ref. [34c,d]. Copyright (2014) American Chemical Society. Copyright (2012) Elsevier. c) The cross-section SEM images of VOG/Ni/Si(100) at 750 and 850 °C and schematics of VOG structural from an ordered morphology to a less vertical morphology with temperature increasing; d) the specific capacitance at 120 Hz as a function of growth temperature; Reproduced with permission from Ref. [34c]. Copyright (2014) American Chemical Society. e) Model electrodes and dynamic diffusion of adsorbed ions over electrode surfaces of HO-GMM, UD-GMM 40, and VOG; Comparison of f) phase angle versus frequency, g) Nyquist plot, and h) electrochemical performance of VO-GMM 40-, HO-GMM 40-, and UD-GMM 40-based ECs. Reproduced with permission from Ref. [37]. Copyright (2021) Elsevier.

this way, the initial Volmer–Weber planar graphitic islands firstly grow on the surface of a catalyst substrate such as Ni. Then the carbon particles collide with each other and push the sp<sup>2</sup> bond upward (Figure 3b),<sup>[34c,d]</sup> eventually forming a VOG morphology.

Miller's team continued to use the VOG as an electrode to study ultrafast response SCs.<sup>[34d,35]</sup> Specifically, the electrochemical performance of the ultrafast SCs was explored, when graphene grown at different temperatures from 600 °C to 800 °C served as electrodes.<sup>[34c]</sup> As shown in Figure 3(c), the VOG prepared at low temperature had a more vertical and open geometric structure. It was more easily accessible to

electrolytic ions. As a result, the specific capacitance of the SC at 120 Hz reached 265  $\mu\text{F cm}^{-2}$  and the phase angle was near  $-85^\circ$  at 120 Hz, which were sufficient for AC filtering. Here, a trade-off effect between the capacitance and impedance phase was observed. The capacitance increased linearly with increasing growth temperature, while the impedance phase decreased with increasing growth temperature. (Figure 3d). Moreover, edge-oriented graphene was grown on a current collector via a 5 min rapid plasma carbonization and deposition process. The SC with edge-oriented graphene showed an attractive phase angle of  $-80^\circ$  at 120 Hz, a high specific area capacitance of 2.34 mFcm<sup>-2</sup>, and a very low ESR of 40 mΩcm<sup>-2</sup>.<sup>[36]</sup>

Importantly, the VOG-based electrodes exhibited excellent frequency performance, compared with horizontally-oriented electrodes and disordered graphene membrane electrodes. It was also verified by electrochemical characteristics and the finite element simulation (Figure 3e–g).<sup>[37]</sup> These results provide new insight into the design of the morphology of electrodes.

The film-like 2D carbon material also showed a good frequency response performance in SCs. Ultrathin

graphene,<sup>[1a,2e,38]</sup> a 2D carbon material with short and accessible channels, also exhibited an excellent frequency response in SCs. As shown in Figure 4(a), an ultrathin graphene nanomesh film (GMF) was prepared by in-situ carbothermal reduction.<sup>[1a]</sup> The GMF could facilitate ion migration and reduce the interfacial impedance due to the high conductivity and the close contact interface between the current collector and electrode material. The rate performance of the SCs was

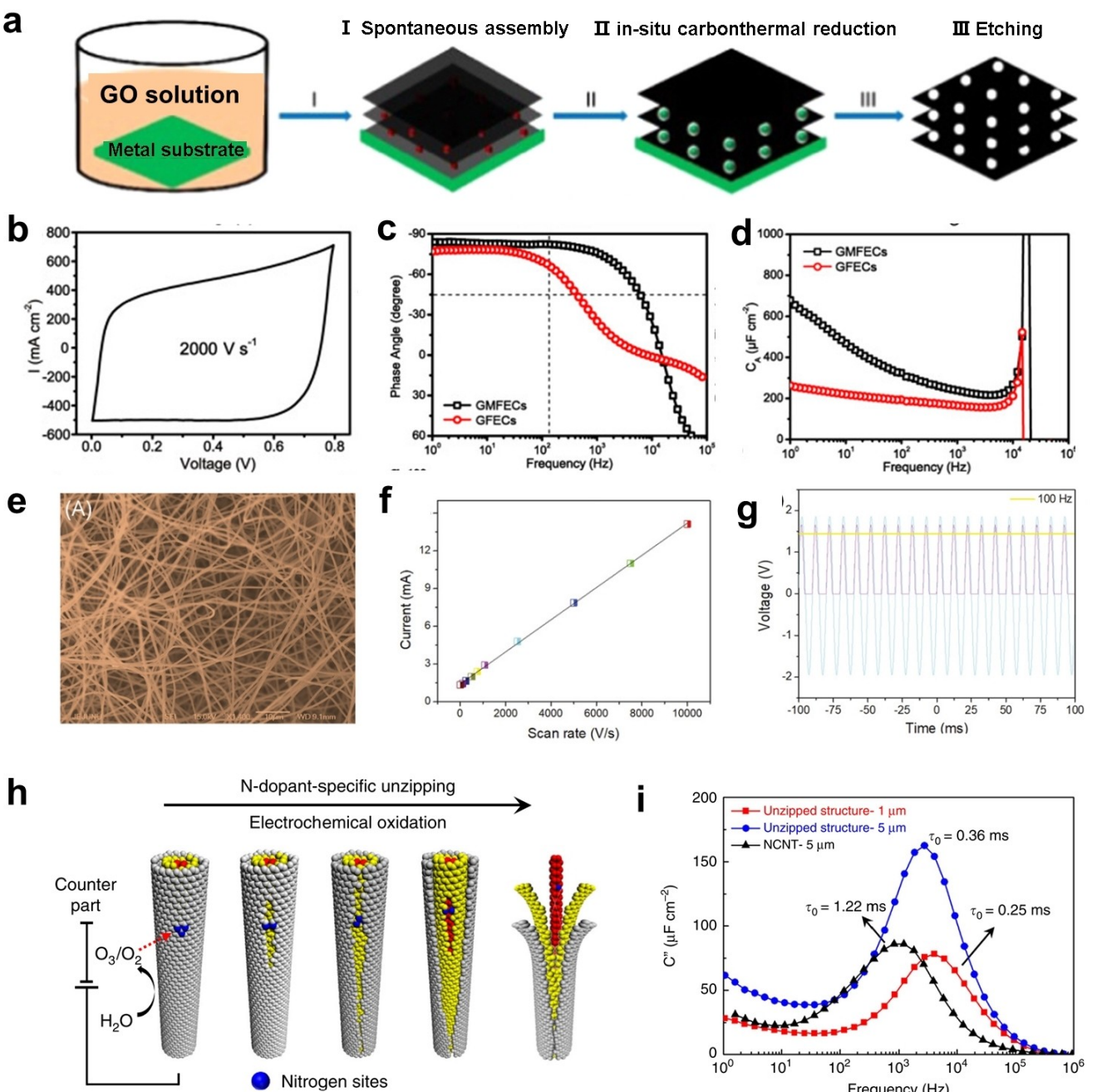


**Figure 4.** a) Schematic illustration of the fabrication of free-standing GMFs; b) CV curve at  $2000 \text{ V s}^{-1}$ ; c) plots of the phase angle versus the frequency and d) Nyquist plots for GMF-ECs. Reproduced with permission from Ref. [1a]. Copyright (2018) Elsevier. e) FE-SEM analysis of the electrospun PVDF; f) Plot of current versus scan rate ( $1\text{--}10\,000 \text{ V s}^{-1}$ ); g) The AC filtering performance of the high-frequency symmetric supercapacitor at 100 Hz; Reproduced with permission from Ref. [39]. Copyright (2021) John Wiley and Sons. h) Schematic illustration of N-dopant-specific unzipping of nitrogen-doped CNTs; i) Bode plot of Ultrahigh-power double layer capacitors with unzipped nanostructure forest electrodes. Reproduced with permission from Ref. [40]. Copyright (2016) The Author(s). Published by Springer.

excellent even under the CV scanning rates up to 2000 V/s (Figure 4b). Importantly, the RC time constant was as fast as 0.36 ms, the impedance phase angle was  $-82.3^\circ$  (Figure 4c), and the specific capacitance reached  $306 \mu\text{F cm}^{-2}$  at 120 Hz (Figure 4d). Moreover, the free-standing carbyne film exhibited excellent rate capacity at the CV scanning rate of up to  $10000 \text{ Vs}^{-1}$  (Figure 4e and f). This is due to the high porosity and good electronic conductivity of the free-standing carbyne film, which is very promising for commercial AEC filtering (Figure 4g).<sup>[39]</sup> Obviously, ultrathin 2D carbon materials with high conductivity and open pore structures are good choices as electrode materials for ultrafast SCs.

Furthermore, the doping of heteroatomic elements (N, P, B) on carbon can enhance the electrochemical performance of carbon-based materials.<sup>[29,41]</sup> It is because that the interaction between heteroatoms and electrolyte ions is favorable for reducing the ionic resistance at the electrode/electrolyte interface. Moreover, doping increases the free charge carrier density of the electrode, thereby increasing the conductivity and contributing to rapid electron transfer.<sup>[28,42]</sup> For instance, compared to the poor frequency response of pure CNTs, the doped CNT-based coin-type SCs exhibited a faster relaxation time constant of 0.2 ms.<sup>[2d]</sup> In another work, doped CNTs displayed a time constant of 0.25 ms, faster than that of undoped CNTs (Figure 4h and i).<sup>[40]</sup> These results validate that the charge storage dynamics could be enhanced by doping at defect sites. Doping is promising for ultrafast SC studies. However, there are still few studies on ultrafast SCs with doped electrodes. Thus, the effect of doping on the frequency response remains to be further explored.

### 3.1.2. Other materials

In addition to carbon materials, 2D pseudocapacitive materials are also considered attractive electrode candidates. For conducting polymers,<sup>[43]</sup> metal organic framework (MOF) derivatives,<sup>[36,44]</sup> transition metal dichalcogenides,<sup>[45]</sup> and two-dimensional transition metal carbides (MXenes),<sup>[2b,46]</sup> they possess high specific surface area, excellent electronic conductivity, and ordered microscope structures.

Since chemical energy storage exists in pseudocapacitors, a higher energy density can be provided while maintaining good power performance. As shown in Figure 5(a),<sup>[47]</sup> the 1T-phase MoSe<sub>2</sub> nanosheets with a rich defect structure were beneficial to the fast adsorption and desorption of electrolyte ions. Meanwhile, the metallic nature of the MoSe<sub>2</sub> nanosheet provided excellent electron transfer. The fast charge dynamics contributed to an unprecedented high-frequency response (up to 10 kHz) and excellent rate performance (Figure 5b).<sup>[47]</sup> Due to their excellent properties of high specific surface area, excellent conductivity, and regular morphology, pseudocapacitive materials are considered as much promising electrode materials for ultrafast SCs. Nowadays, There are few studies on pseudocapacitive electrodes.

Moreover, the mass load of electrode materials influences the electrochemical performance by affecting the ion trans-

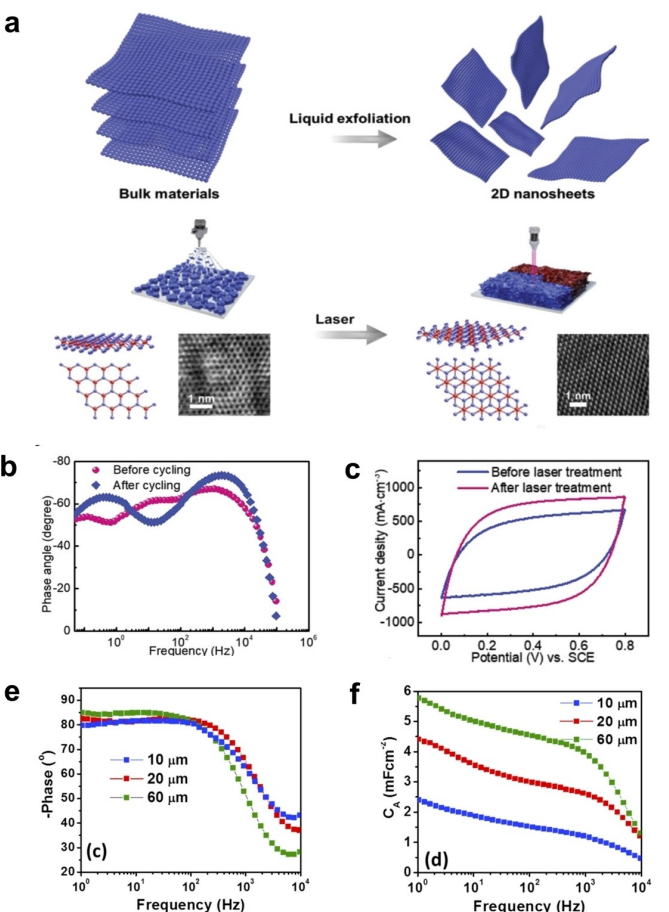


**Figure 5.** a) Fabrication route for laser-processed 1T MoSe<sub>2</sub> electrodes; b) Impedance phase angle versus frequency before and after cycling of MoSe<sub>2</sub> electrodes. Reproduced with permission from Ref. [47]. Copyright (2018) John Wiley and Sons. Comparison of the three electrodes in the aqueous electrolyte of e) the phase angle vs. frequency and f) areal capacitance vs. frequency. Reproduced with permission from Ref. [49]. Copyright (2017) Elsevier.

portation distance. Increasing the mass load (or a thick electrode) can significantly improve the energy density.<sup>[2e,4,42]</sup> However, the ion diffusion length across a thick electrode driven by charges becomes longer, which will result in a slower dynamic response.<sup>[48]</sup> Taking carbon fiber aerogel electrode as an example, the electrode thickness effect on the capacitance and the impedance phase was studied.<sup>[49]</sup> As shown in Figure 5(c and d), the characteristic frequency at the  $-45^\circ$  phase diminished from 4.1 kHz to 1.3 kHz when the electrode thickness increased from 10  $\mu\text{m}$  to 60  $\mu\text{m}$ . The areal capacitances of the 10  $\mu\text{m}$ -, 30  $\mu\text{m}$ -, and 60  $\mu\text{m}$ -electrodes were 1.51, 2.98, and 4.50  $\text{mF cm}^{-2}$ , respectively. Obviously, a thick electrode with high mass loading increased the energy density, but caused a loss of rate performance at the same time. The right is best. It is better not to sacrifice the capacitance of SCs in pursuit of an excessively fast response.

In summary, the morphological design of electrode materials is crucial. Good electrodes for ultrafast SCs should possess high conductivity and a regular open pore structure to achieve rapid charge transfer and ion diffusion. Currently, VOG, array

CNTs, and pseudocapacitive materials with high conductivity are prospective electrode materials. In addition, the energy density of the SC should be maximized while maintaining a good frequency response. Therefore, the specific surface area of electrode materials should be increased moderately to store more charge.

### 3.2. The structure of the current collector

#### 3.2.1. Type of current collectors

The roles of the current collector are mainly as follows: first, to act as a carrier of the powdered electrode material; second, to collect and output the current generated by the active material or to feed the current to the active material. As a result, the current collector is required to have good conductivity, stable electrochemical properties, and high mechanical strength. It provides channels for electron transport during charge-discharge. Thus, the current collector can help to realize the minimum contact electron impedance and promote the charge dynamics of SCs.

Generally, a current collector with higher conductivity is more conducive to improving the electrochemical performance of the device. Moreover, the surface modification of the current collector will affect the electrochemical performance due to the difference in interface impedance, even for current collectors with the same material. As shown in Figure 6(a), Linda's team<sup>[30]</sup> compared the frequency response performance of three treated current collectors: polished stainless steel, roughened stainless steel and roughened & gold coated stainless steel. Among them, roughened & gold-coated stainless steel showed the best rate performance (Figure 6b). The AC specific capacitance reached  $601 \mu\text{F cm}^{-2}$  at 120 Hz and the impedance phase angle reached  $-81^\circ$ , which were as good as those of other works with an Au/Al foil current collector<sup>[2e]</sup> (Figure 6c). This was mainly due to the ultrahigh electrical conductivity of the Au current collector,<sup>[1a,2e,7,25e,50]</sup> which promoted electron migration and reduced internal resistance. This is further proved by the disappearance of the semicircle in the high-frequency region of the EIS. Similarly, carbon paper current collectors were also favored.<sup>[51]</sup> Moreover, the frequency performance of the SC with roughened stainless steel as the current collector was better than that of the SC with polished stainless steel as the current collector.<sup>[30]</sup> This was because that the rough current collector surface offered a larger contact surface with active materials, which contributed to the low interface impedance.

The morphology of current collectors also affects the electrochemical performance. A 3D porous foam current collector can provide barrier-free ion transport channels and ensure sufficient contact between electrode materials and the current collector in three dimensions. As a result, it is a promising choice for ultrafast SCs. As shown in Figure 6(d), Ni foam increased the proportion of carbon-metal contact, reduced the proportion of carbon-carbon contact, and led to lower contact resistance.<sup>[53]</sup> For planar current collectors such as

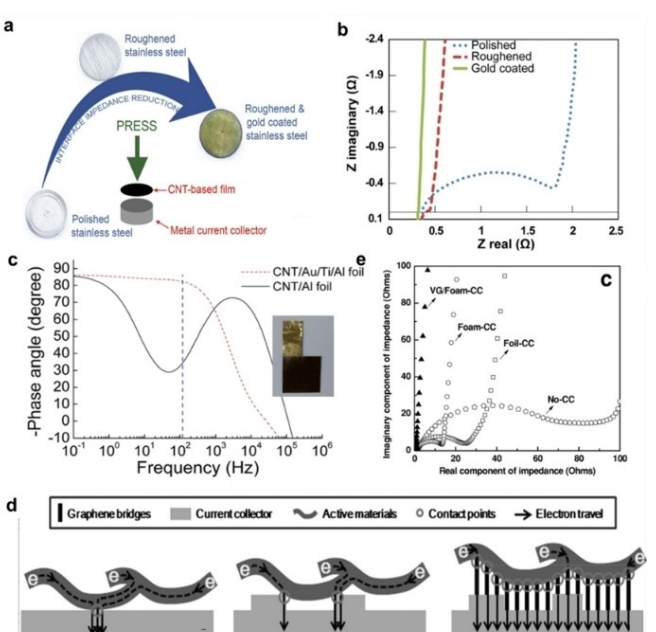


**Figure 6.** a) The schematic diagram of polished, roughed, and gold-coated stainless steel current collectors; b) Nyquist plots of three current collectors; Reproduced with permission from Ref. [30]. Copyright (2015) American Chemical Society. c) Bode phase plots of CNT supercapacitors with and without Au coatings on the Al foil current collectors. Reproduced with permission from Ref. [2e]. Copyright (2015) Royal Society of Chemistry. d) Schematic illustration of electron transport between active materials and Foil-CC, Foam-CC, and VG/Foam-CC; e) Nyquist plots for No-CC, Foil-CC, Foam CC, and VG/Foam-CC working electrodes. Reproduced with permission from Ref. [52]. Copyright (2013) John Wiley and Sons.

Al foil, the contact between the electrode material (carbon) and the current collector is not sufficient, and binders are needed. In Figure 6(e), non-conductive binders hindered the electron transfer between carbon and carbon, so the charge transfer resistance was as high as  $25 \Omega$ .<sup>[52]</sup> When graphene was coated on Ni foam as a current collector (VG/Foam collector), the contact points further increased and the electron transfer was optimized. As expected, the charge transfer impedance of the VG/Foam collector was less than  $1 \Omega$  compared with the  $13 \Omega$  of Ni foam.<sup>[52]</sup> Obviously, the 3D current collector was conducive to minimizing the electron impedance under the same conditions.

In conclusion, a 3D high conductivity current collector would be a good choice for ultrahigh-frequency SCs, such as 3D Al foam or 3D carbon paper.

#### 3.2.2. The interface between electrode materials and the current collector

The electrode-collector interface affects the electrochemical performance by affecting interface impedance and charge transfer. Typical SCs usually employ thick electrodes with a heterojunction interface<sup>[29,54]</sup> by spanning, coating, or other physical methods.<sup>[2e,55]</sup> Although a thick electrode is beneficial for high energy density, the high impedance restricts the frequency response of SCs. A small interface resistance prompts

excellent ohmic contact to enhance the charge transfer. As a result, the in-situ growth of electrode materials on the current collector surface was explored to acquire a small interface resistance.<sup>[26,34b,56]</sup> As shown in Figure 7(a), both the low interfacial impedance and the ultrafast response of SCs were achieved by the in-situ coating active carbon layer on the sketch of 3D Al foam<sup>[26]</sup> or by the growing VOG in situ on Al substrate.<sup>[34b]</sup> According to the spherical-aberration corrected transmission electron microscope (ACTEM) characterization (Figure 7b-d), the atomic interaction of C-Al in the interface was obtained. This contributed to excellent ohmic coupling and ultrafast frequency response of SCs in the ionic liquid electrolyte.<sup>[26]</sup>

From the analysis of charge dynamics in Section 2, the interface impedance reflects the charge transfer speed and determines the response speed of the SC. For ultrafast SCs, the interface impedance is very small ( $< 0.1 \Omega$ ), as shown by the absence of the semicircle at high frequency in the Nyquist plot. The interfacial impedance is influenced by the electrode-current collector interface structure in addition to the electrode material and the current collector. A tightly bonded electrode-current collector interface can be obtained by growing active materials in-situ on the current collector surface. Clearly, this helps to reduce the interface impedance and achieve an ultrafast response. However, the quantitative influence of each component of SCs on the interface impedance needs to be further investigated.

### 3.3. Electrolytes

As shown in Figure 8, the energy density of an SC is proportional to the square of the working voltage of electrolytes, based on  $E = \frac{1}{2}CU^2$ .<sup>[57]</sup> The existing three electrolytes (aqueous solution, organic electrolyte, and ionic liquid) differ greatly in the voltage window, which is 0.2–1 V, up to 2.7 V and 3–6 V, respectively.<sup>[58]</sup> The electrolytes determine the working voltage and temperature of SCs. The physical properties of electrolytes,

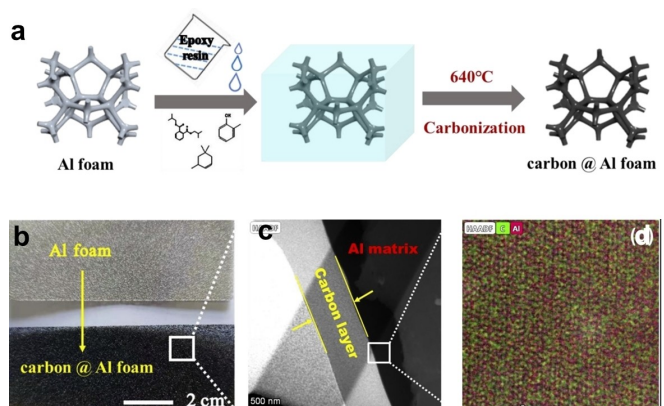


Figure 7. a) Schematic diagram of the preparation route of carbon-coated Al foam; b) ACTEM image of the Al/C interface; c) ACTEM-EDS image of the Al/C interface; d) The HAADF-ACTEM-EDS image of the Al/C interface; Reproduced with permission from Ref. [26]. Copyright (2021) American Chemical Society.

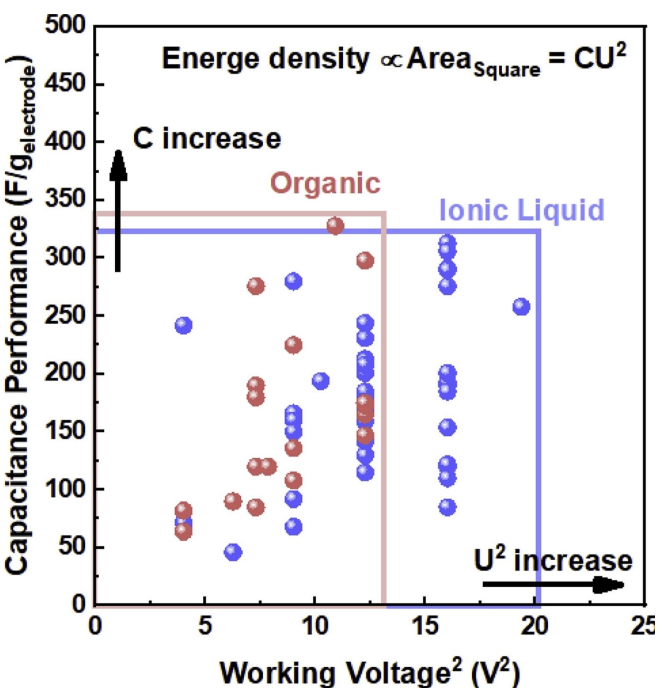


Figure 8. SC performance by combining sp<sup>2</sup> carbon materials and two kinds of electrolytes. The advantage of a high working voltage appears. Reproduced with permission from Ref. [57]. Copyright (2019) Elsevier.

including ionic size, conductivity, and viscosity, affect the charge dynamics of SCs by influencing the diffusion impedance.

#### 3.3.1. Aqueous electrolytes

Fast electron transfer and ion diffusion are determining factors for an ultrafast response. Owing to the small size of ions (0.2–0.4 nm), high ionic conductivity, and low viscosity,<sup>[58b,59]</sup> aqueous electrolytes are mainly used for ultrafast-response SCs. The aqueous electrolytes commonly used in current ultrafast response studies of SCs include acidic electrolytes such as 1 M H<sub>2</sub>SO<sub>4</sub>,<sup>[9c,42,43,60]</sup> neutral electrolytes such as 1 M Na<sub>2</sub>SO<sub>4</sub>,<sup>[29]</sup> and alkaline electrolytes such as KOH solution.<sup>[1c,2a,20b,41a,46a,51b,55,61]</sup> For example, flexible micro-supercapacitors (MSCs) with porous conducting poly(3,4-ethylenedioxythiophene) (PEDOT) electrodes exhibited remarkable performance in a 1 M H<sub>2</sub>SO<sub>4</sub> aqueous electrolyte. Specifically, an ultrahigh scan rate of up to 500 Vs<sup>-1</sup> was achieved, and a cutoff frequency was 400 Hz at an impedance phase angle of 45°.<sup>[43]</sup> Such good frequency response performance was attributed to the electrode material and the aqueous electrolyte. To be specific, the high conductivity and low viscosity of the aqueous electrolyte played an important role in promoting ion migration. And high conductivity electrodes enhanced the electron transfer.

The KOH solution has high ionic conductivity (0.6 Scm<sup>-1</sup> for 6 M KOH at 25°C) and high compatibility with the Ni current collector.<sup>[62]</sup> Therefore, the KOH solution is the most commonly used among various alkaline electrolytes. Based on a 3 M KOH

aqueous electrolyte of 1 V, the SC with vertically oriented NiTe<sub>2</sub> nanosheet/Ni foam electrodes exhibited a fast RC time constant of 1.01 ms.<sup>[61]</sup>

Notably, corrosion-resistant electrodes or current collectors should be used in acidic electrolytes or alkaline electrolytes. Here, carbon electrodes can remain stable in acidic or alkaline electrolytes at low temperatures. However, elevating the temperature may result in the functionalization of carbon electrodes to introduce –OH, –C=O, and –COOH groups. In particular, the current collector materials (mostly Al, Cu, and Ni) are susceptible to corrosion in acidic or alkaline electrolytes. Stainless-steel current collectors are resistant to corrosion in acidic or alkaline electrolytes. However, it is acceptable in industries but rarely used in fundamental studies because of their low conductivity.

In summary, making the electrode resistant to acid or alkaline electrolyte corrosion for a long time in practical applications is still a challenge. On the other hand, the low working voltage (0.2–1 V) of aqueous electrolytes limits the energy density of SCs.

### 3.3.2. Organic electrolytes

Organic electrolytes are the most extensively applied commercial electrolytes today. They consist of solvents and salts and, exhibit a higher voltage window (up to 2.7 V) than aqueous electrolytes. Solvents such as acetonitrile (AN), propylene carbonate (PC), and γ-butyrolactone (GBL) are used to dilute the salts and increase the mobility of the ions. To date, organic electrolytes are widely used in the field of ultrafast SCs. Among them, 1 M TEABF<sub>4</sub>/AN<sup>[2d,25d,33,34b,38a,39,49,55b,63]</sup> is the most widely adopted because of its high conductivity and window voltage. Specifically, the 1 M TEABF<sub>4</sub>/AN SC had a working voltage of 2.5 V, achieving an ultrafast response of 0.6 ms and an impedance phase of up to 82.2°.<sup>[2e]</sup> When using Ketjen black as the electrode material, the SC with 1 M TEABF<sub>4</sub>/AN showed a high specific capacity of 574 μF cm<sup>-2</sup> at 120 Hz.<sup>[64]</sup> Additionally, PC is also employed as a solvent in ultrafast SCs. PC contributes to a higher voltage window than that of AN, although it increases the viscosity of electrolytes.<sup>[65]</sup> For example, a SC with onion carbon electrodes and the TEABF<sub>4</sub>/PC electrolyte operated at voltages up to 3 V, which showed an ultrafast frequency response of 26 ms.<sup>[7]</sup>

Moreover, flexible SCs with ultrafast response can be achieved by employing gel organic-based electrolytes, including 3 M H<sub>2</sub>SO<sub>4</sub>/PHEMA/PVA gel,<sup>[2b]</sup> H<sub>2</sub>SO<sub>4</sub>/PVA gel electrolyte,<sup>[9d,46b,56,63a,66]</sup> and TEAOH-PVA electrolyte.<sup>[35b]</sup> Flexible SCs for electronics may be a hot topic in the future, which will be discussed in chapter 4 of this review.

Organic electrolytes cannot work properly at high temperatures due to their tendency to volatilize and decompose. However, AC filtering is often required to operate at high temperatures (50–120 °C). Therefore, electrolytes that can withstand high temperatures should be further explored.

### 3.3.3. Ionic liquid electrolytes

The ionic liquid (IL) electrolyte consists of a type of organic cation and a type of inorganic anion. The interaction of two pure ions is weak, so ILs remain in a liquid state at ambient temperature. Compared to aqueous and organic electrolytes, ILs possess a high voltage window (3–6 V)<sup>[28,67]</sup> due to the high concentration of conductive ions. Hence, SCs with IL electrolytes always exhibit a high energy density, which is of great significance to reduce the SC volume. Moreover, ILs have the advantages of a wide liquid temperature range, nonvolatile, nonflammable, and nontoxic. These features are all highly desirable for AC filtering applications. Therefore, researchers have begun to turn their attention to ionic liquid ultrafast response SCs.<sup>[9a,34d,68]</sup>

Notably, the ion pairs in ILs are easily formed, which can increase the viscosity and decrease the ionic conductivity of ILs. Clearly, this will restrict the ion diffusion required for ultrafast response. Therefore, it is essential to break the ion pairs to increase ion mobility. Qian's team reported for the first time that the ultrafast response of SCs can be achieved with the pure IL electrolyte of EMIBF<sub>4</sub> at 4 V.<sup>[26]</sup> The as-made coin-type SC and the pouch-type SC implemented ultrafast responses of 1.5 ms and 0.5 ms, respectively. The response time was even excellent compared to many cells with aqueous electrolytes or organic electrolytes. And they could stabilize the voltage for the LED in the AC filtering circuit. It was considered that the ion interaction of ILs near the electrolyte-electrode interface was different from that in the bulk phase. Thus, the presence of free ions was essential to rapid diffusion. Such deduction was supported by the experiments with DTG (as shown in Figure 9a–c). In detail, DTG curves showed that the melting point of ILs mixed with carbon materials was lower than that of pure ILs. The trend became significant as the ratio of carbon materials to ILs increased, validating the increase in the ratio of free ions near the interface. At the microscopic scale, there were π bonds on the heterocyclic rings of cations in ILs, which tended to π–π interactions with sp<sup>2</sup> hybridized carbon. Such enhanced bonding at the interface resulted in the movement of ions far from their bulk phase. Meanwhile, Feng's team studied the molecular dynamics simulation of ILs in SCs.<sup>[69]</sup> They proposed that, ions in high-concentration ILs could form a 'cage' configuration due to the interaction and the size difference between anions and cations. The 'cage' configuration was called 'bound' ion pairs. Many free ion pairs also existed in ILs, which was helpful to realize the ultrafast response of SCs (Figure 9d and e). These encouraging results suggested that the SCs with pure IL electrolyte performed not as badly as expected for frequency performance.

In summary, ILs show great potential in ultrafast SCs based on both experimental and theoretical calculations.

### 3.3.4. Other electrolytes -water in salt electrolytes

Water-in-salt electrolytes (WiSEs) show a wide electrochemical stability window (ESW) due to a reduction in the number of

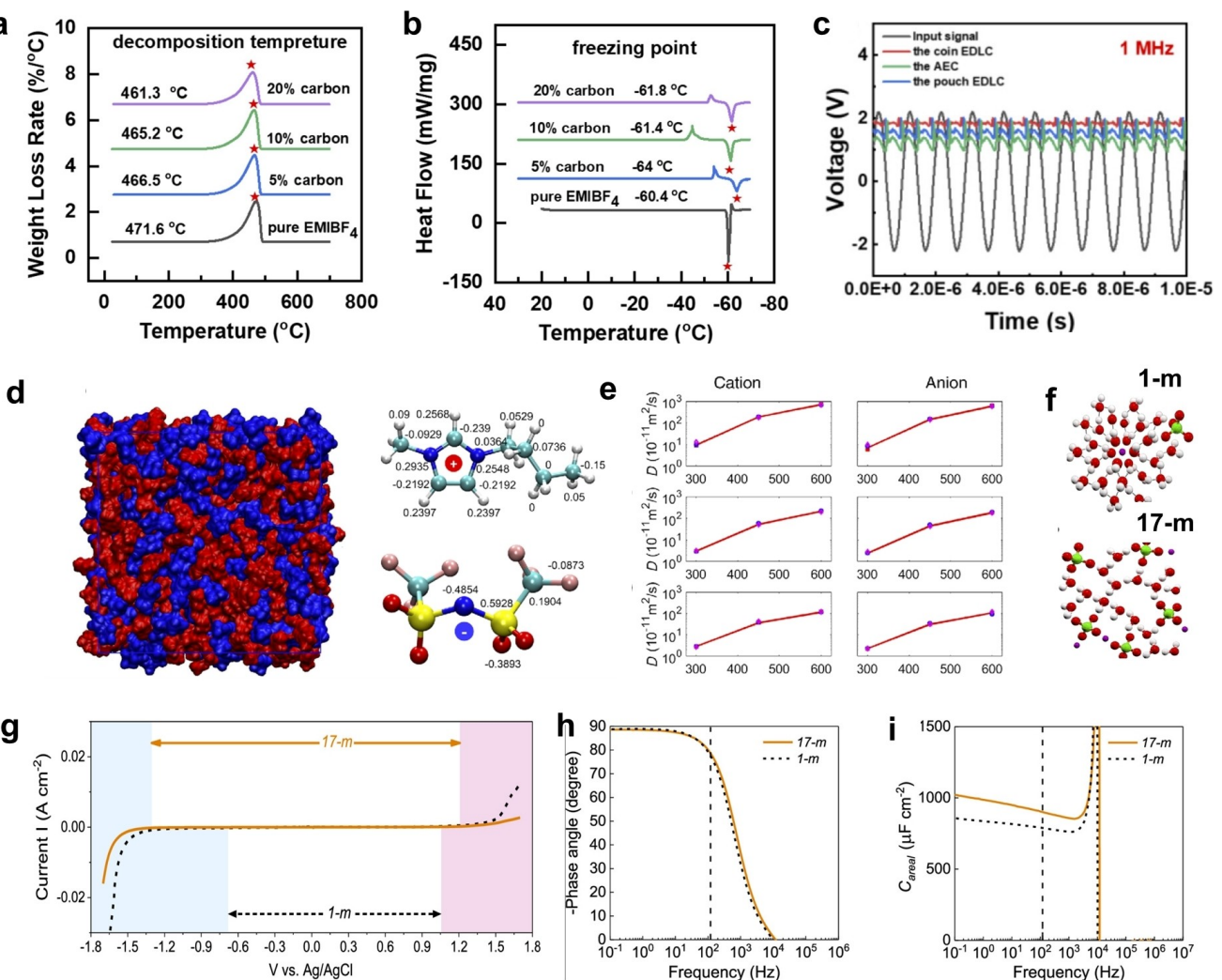


**Figure 9.** a) Decomposition peak of ILs with carbon in DTG (air atmosphere, from ambient temperature to 700 °C at a rate of 10 K/min); b) Freezing point of ILs with carbon in DSC (from 20 °C temperature to -70 °C); c) DC output signals from the AC filtering circuit with AC signals at a frequency of 1 MHz. Reproduced with permission from Ref. [26]. Copyright (2021) American Chemical Society. d) Molecular dynamics simulation of bulk RTIL [Bmim][TFSI]; e) The influence of MD simulation box size on the free-ion percentage, the diffusion coefficient of ions in the free state. Reproduced with permission from Ref. [69a]. Copyright (2019) APS Physics. f) Solvation shell structures of low- (1 M) and high-concentration (17 M) NaClO<sub>4</sub>-based aqueous electrolytes; g) Determination of the ESW of the 1 M and 17 M NaClO<sub>4</sub> SCs. Reproduced with permission from Ref. [58a]. Copyright (2021) American Chemical Society.

free water molecules.<sup>[70]</sup> Therefore, WiSEs are a promising candidate for electrolytes of energy storage devices. For example, the viscosity of the 17 M NaClO<sub>4</sub> is 5 times higher than that of the 1 M NaClO<sub>4</sub>. Surprisingly, the SC with 17 M NaClO<sub>4</sub> exhibited a faster frequency response as shown in Figure 8f-i. As a comparison, there was a high phase angle ( $-\Phi = 78.7^\circ$  vs  $77.6^\circ$  at 120 Hz), a high areal capacitance (901 vs  $789 \mu\text{F cm}^{-2}$  at 120 Hz), and a low ESR (0.24 vs. 0.33 Ω). Evidently, it was considered that ion transport in high-concentration WiSEs (17 M NaClO<sub>4</sub>) was comparable to that in a dilute electrolyte (1 M NaClO<sub>4</sub>). This unexpectedly excellent performance may be attributed to the unique biphasic structure of water and ion-aggregate networks in the WiSEs.<sup>[58a]</sup>

In summary, for replacing the AC filtering application of AECs, aqueous electrolytes and organic electrolytes may be excluded because they cannot withstand high temperature. But

IL electrolytes and WiSEs show prospects in the field of high temperature.

#### 4. The Configuration of Ultrafast Response Supercapacitors

With the in-depth study of ultrafast SCs, various electrode materials have been explored from common carbon materials (including activated carbon, graphene, and CNTs) to organic polymer materials, metal oxide materials, and metal sulfide materials. Although rapid advances in ultrafast response have been achieved, the influence of device configurations remains to be explored. In particular, SC configurations are important

for AC filtering. Here, we classify and discuss the configurations of the ultrafast SCs studied.

#### 4.1. Symmetric ultrafast response SCs

At present, most of the ultrafast SCs studied are symmetric configurations. Here, we divide symmetric SCs into micro-supercapacitors (MSCs), coin-type SCs, and extended SCs according to their size.

##### 4.1.1. Microsupercapacitors

For ultrafast response SCs expected to be applied in electronics, they are required for good integration.<sup>[47]</sup> MSCs are mainly fabricated on a chip and integrated into thin-film electronics. Therefore, the configuration of MSCs is beneficial for a shorter interconnection distance and more compact distribution.

Finger planar interdigitated MSCs are the main MSC configuration.<sup>[7,9a,d,37,43,46b,47,50b,56,65,71]</sup> As shown in Figure 10(a), the preparation of finger MSCs requires no membrane and shell. First, the insulating area needs to be fabricated by photolithography of the current collector, and then the electrode

material is deposited in situ. This configuration can maximize the accessible surface area of active materials and show the original characteristics of the electrode material.<sup>[46b]</sup> Specifically, finger MXene MSCs achieved high volumetric capacitance ( $30 \text{ F cm}^{-3}$  at 120 Hz), high rate capability ( $300 \text{ Vs}^{-1}$ ), and a short  $\tau_0$  of 0.45 ms (Figure 10b).<sup>[46b]</sup>

In addition, 10 integrated MSCs fabricated on a 4-in  $\text{SiO}_2/\text{Si}$  wafer, which worked at a 6 V voltage window. Moreover, it showed good rate performance with a nearly rectangular shape at a  $300 \text{ Vs}^{-1}$  scanning rate (Figure 10c).<sup>[46b]</sup> Meanwhile, the carbon membrane-based finger-interdigitated MSCs showed a good frequency response for 120 Hz AC filtering.<sup>[71c]</sup>

Interestingly, the ultrafast response of flexible MSCs can also be achieved by using gel organic-based electrolytes.<sup>[9c,38b]</sup> Wu's team adopted a PET flexible substrate and  $\text{H}_2\text{SO}_4/\text{PVA}$  gel electrolyte to fabricate MSCs (Figure 10g).<sup>[38b]</sup> The flexible MSC showed an impedance phase of  $-75.6^\circ$  and a high energy density of  $2.5 \text{ mWh cm}^{-3}$ , which was compatible with the rapid development of portable electronics.<sup>[38b]</sup>

Obviously, based on the competitive performance, MSCs may be able to replace bulky AECs. Moreover, MSCs can be scaled up, allowing for the rapid integration of hundreds to thousands on a substrate.<sup>[46b]</sup> This will contribute to high energy density. For further study, the MSC configuration may be

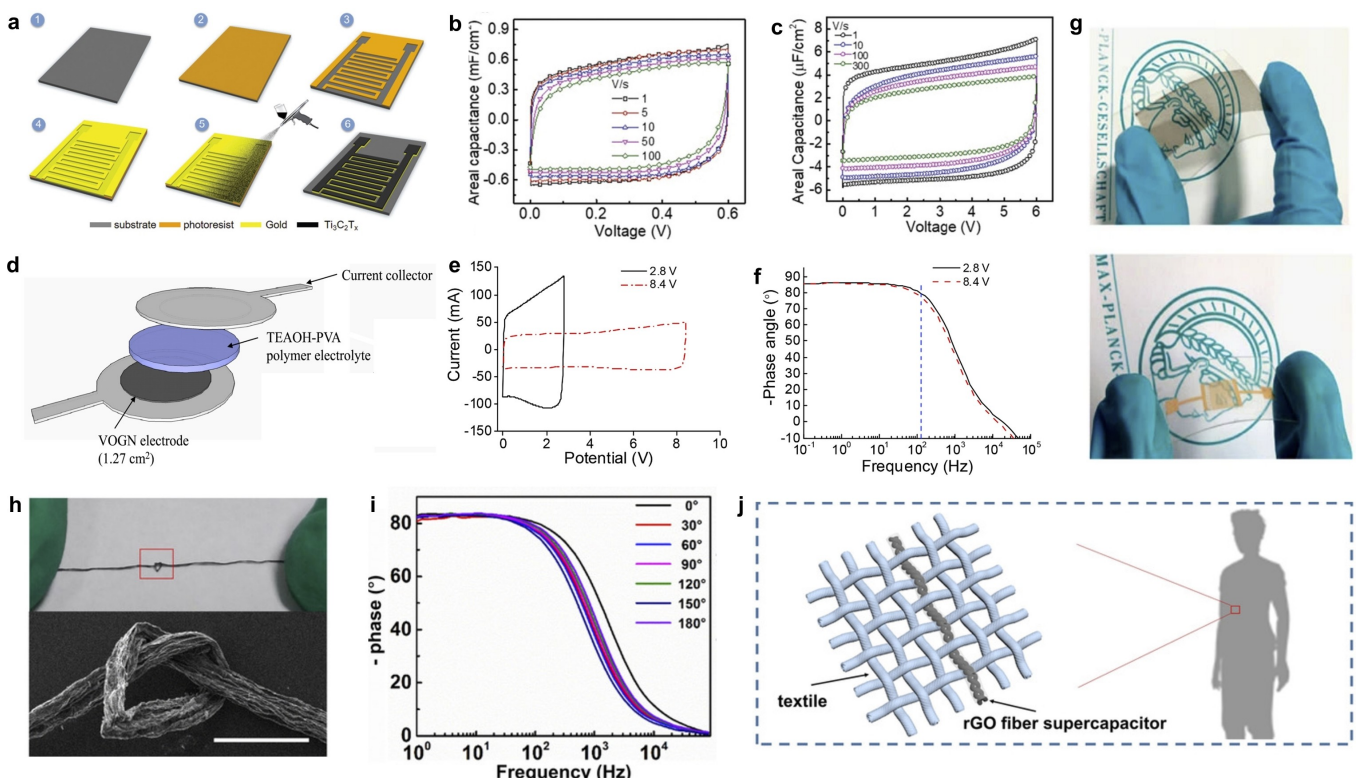


**Figure 10.** a) Schematic illustration of the fabrication process of MXene MSCs; b) CV curves of Ti<sub>3</sub>C<sub>2</sub>T<sub>x</sub>-0.3 μm MSC; c) CV curves of 10 MSCs connected in series at various scan rates; Reproduced with permission from Ref. [46b]. Copyright (2019) John Wiley and Sons. d) Schematic diagrams of a solid-state sandwich design SC Reproduced with permission from Ref. [35b]. Copyright (2016) Elsevier. e) Cyclic voltammograms measured at 100 Vs<sup>-1</sup> and f) phase angle as a function of the frequency of single- and three-cell SCs. Reproduced with permission from Ref. [64]. Copyright (2017) Elsevier. g) The MPG film transferred onto the PET substrate with and without Au collectors; Reproduced with permission from Ref. [38b]. Copyright (2013) The Author(s). Published by Springer Nature. h) The optical and SEM images of a knot in the rGO fiber; i) The phase angles of SCs-3 which is bent to various angles (0°, 30°, 60°, 90°, 120°, 150° and 180°); j) The potential application of rGO fiber SCs for wearable applications. Reproduced with permission from Ref. [66b]. Copyright (2019) John Wiley and Sons.

optimized by increasing interdigital fingers or decreasing the interspaces between the electrodes.<sup>[38b]</sup> Considering the rapid development of flexible electronics, flexible SCs for AC filtering may be a hot topic in the future.

#### 4.1.2. Coin-type SCs

As a typical configuration (Figure 10d), because of small sizes and simple assembly, coin-type SCs are convenient for evaluating electrochemical performance. They, therefore, were initially widely adopted for ultrafast response SCs.<sup>[1a,c,2a,d,29,33,34d,35b,37,38,42,51a,55a,61,63a,64]</sup> Coin-type SCs are all the sandwich configuration, which consists of the electrode-electrolyte-electrode in a sequence and is named "sandwich". Sandwich SCs have the advantage of simple manufacturing. Minutely, highly conductive electrodes with 3D edge-oriented graphene were packed into a coin cell and showed high-frequency performance. The characteristic frequency of the coin cell at  $-45^\circ$  was up to 22 kHz and the electrode capacitance density was  $0.37 \text{ mF cm}^{-2}$  at 120 Hz.<sup>[38a]</sup> Multiple coin SCs can also be connected in series to achieve high operating voltage of ultrafast SCs. Kim's team<sup>[64]</sup> demonstrated that three coin-SCs connected in series exhibited an excellent phase angle of  $80^\circ$  and worked at 8.4 V (Figure 10e and f).

However, coin-type SCs with a thick shell can yield an extra resistance compared to other configuration SCs, which will retard the response speed of SCs.

#### 4.1.3. Extended flexible SCs with sandwich structures

To date, general studies of AC filtering have focused on small devices. Large or extended SCs are rarely reported, probably owing to the increased difficulty in fabricating technology. However, extended flexible SCs, including film-like SCs<sup>[9b,26,39,60,66a]</sup> and fiber-shaped SCs,<sup>[2b,66b,72]</sup> have the advantages of high energy density and flexible bending.

The film-like flexible SCs are all sandwich structures. The pouch-type SC, one type of film-like flexible SC, has the characteristics of a large area and flexibility and an adjustable number of electrodes. This configuration contributes to lower contact resistance, high capacitance, and high energy density. Zhang demonstrated the effect of the stacked electrode number on pouch-SC performance. When increasing the number of electrode sheets, the response time would not dilate and the capacitance would positively rise.<sup>[26]</sup>

Ultrathin printable graphene SCs on an ultrathin poly(ethylene terephthalate) substrate is a film-like flexible SC, which exhibited prominent rate performance and AC line filtering.<sup>[66a]</sup> Importantly, the flexible SC with CNT thin-film electrodes and ionic-liquid-based polymer gel electrolyte exhibited a high-frequency response. Compared to other works, it had a much higher energy density ( $0.42 \mu\text{Wh cm}^{-2}$ ).<sup>[9b]</sup> This benefited from an IL-based gel electrolyte with a high working voltage (3 V), consistent with the previous conclusion.

Moreover, the symmetric fiber-shaped SC was constructed from two twisted reduced graphene oxide (rGO) fibers with gel electrolytes. It exhibited a short RC time constant (approximately 0.32 ms) and good AC filtering properties ( $-82.3^\circ$  at 120 Hz).<sup>[72]</sup> In addition, the flexible fiber-shaped SC with rGO fibers realized an excellent frequency response (0.24 ms) in bending and folding states (Figure 10h and i).<sup>[66b]</sup>

Clearly, flexible SCs show the potential for high-frequency applications such as wearable devices (Figure 10j). And developing high-voltage electrolytes is a promising method to get ultrafast flexible SCs with high energy density. In the future, optimizing the SC configuration will be an orientation to improve the electrochemical performance (frequency response speed, high energy density, and high specific capacitance).

#### 4.2. The asymmetric ultrafast response SCs

Asymmetric hybrid SCs not only have high power density and long cycle life, but also have high energy density close to the battery. Recently, an asymmetric SC with an rGO/MXene composite film as a negative electrode and a PEDOT:PSS-based film as a positive electrode was studied. It displayed an outstanding frequency response, of which the  $\tau_{\text{RC}}$  at 120 Hz was 0.2 ms.<sup>[73]</sup> Moreover, asymmetric SCs could be alternately stacked assembly for compact integration, and there was no loss in frequency response performance.

At present, the high-frequency response SCs studied are mainly symmetric configurations, while there are few studies on asymmetric SCs. In our opinion, hybrid SCs will be an important direction for practical frequency applications due to their very high energy density.

#### 5. Perspective

Ultrafast response SCs have made great progress, while the specific capacitance of ultrafast SCs is much better than that of AECs. Importantly, high-frequency SCs show great promise for applications such as filtering electronic devices, frequency regulation of power grid systems, and smart portable wearable devices. For AC filtering, the devices should meet the requirements of response time, impedance phase angle (at 120 Hz), capacitance, operating temperature range, and operating voltage. As shown in Figure 11, advances in ultrafast response SCs are summarized from five perspectives. Besides, the distance from research status to the practical application of AC filtering is evaluated. Obviously, there exists a big gap between AECs and SCs in terms of the operating temperature and operating voltage.

However, although good progress in ultrafast SCs has been made thus far, an in-depth study remains to be advanced. Here, we present the following outlook on the development of ultrafast response SCs.

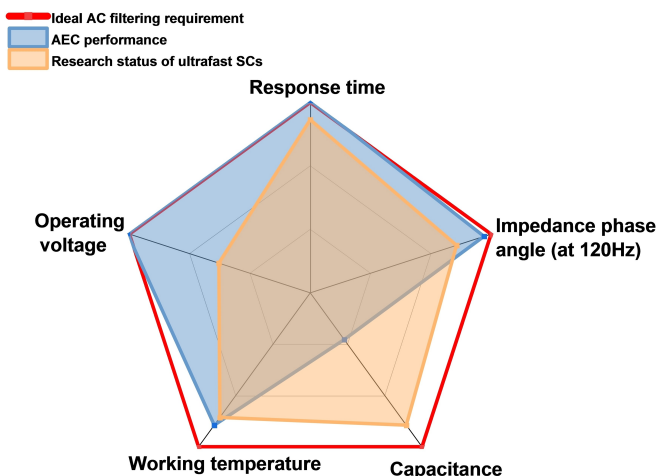


Figure 11. Summary and comparison for ideal AC filtering requirements, existing AECs performance, and research status of ultrafast SCs.

### 5.1. Mechanism exploration

At present, the studies on ultrafast response are still superficial, most of them are discussed based on macroscopic electrochemical tests. Thus, a deeper mechanism analysis remains to be studied. Specifically, the charge dynamics in the fast response process and the potential barriers all required in-depth exploration. Meanwhile, it is difficult to capture real-time internal changes during the ultrafast response of SCs. Fortunately, it may be possible to explain the response mechanism with the development of advanced characterization and computational simulation technologies.

### 5.2 Matching design of the electrode and electrolyte

Increasing the specific surface area of electrode materials in SCs is a common way for high specific volume capacitance. Apart from that, ultrafast SCs should care about the pore structure inside electrodes to ensure fast ion diffusion at high frequency. For too small pores, the inaccessibility of electrolyte ions will result in a partially ineffective specific surface area of electrodes. And the interaction between the pore channels and the ions will become a large barrier for ion diffusion. Similarly, it is also unable to achieve fast ion diffusion in a zig-zag channel, compared to a straight channel. Apparently, hierarchical pores with a fully interconnected structure would be an ideal choice.

In view of electrolyte-ion diffusion in fixed pores, ion size should be of great concern. Small ions always exhibit far higher diffusion rates than large ions driven by potential. In addition, the viscosity and ion conductivity of electrolytes will both be key issues, taking into account ion diffusion and electron transfer.

### 5.3. Electrolytes study for various temperature applications

Because of the limitation of solvent volatile points, most aqueous electrolyte-based SCs and organic electrolyte-based SCs can only work below 80 °C. In the current standard, the upper temperature of organic electrolyte-based SCs in the accelerated aging test is always set to 65 °C. However, AECs can work at high temperatures of 100–120 °C. In comparison, IL-based SCs can work at high temperatures of up to 120–150 °C, due to the high intrinsic chemical stability of ILs. Additionally, the nonflammability of ILs exhibits high security, which is attractive for circuit applications. Thus, it is feasible to develop suitable IL electrolytes for ultrafast SCs in the future.

However, on the one hand, the increasing working temperature challenges the electrolyte stability, which will shorten the lifetime of the device. Especially, the coupling of the high temperature and high voltage will exhibit a serious impact on the stability of the AC filtering device. As a result, the ripple current at a maximal temperature in AC filtering circuits should be controlled. Obviously, much work should be done for proper evaluation over a wide working-temperature range.

On the other hand, ILs often have a limited low-temperature window. For instance, EMIBF<sub>4</sub>, a 4 V electrolyte, works only at –10 °C. Further decreasing the operating temperature would result in the freezing of EMIBF<sub>4</sub> or at least at an unstable working zone. Therefore, in our opinion, mixing ILs with different anions or cations is an effective way, which can break the ion pairs of ILs and extend the temperature range.

### 5.4. The development of high-voltage ultrafast supercapacitors

The main purpose of developing ultrafast SCs is to increase the volumetric energy density of the filters in space-constrained circuits. However, there exists a limitation to using liquid electrolyte-based SCs for AC filtering in high-voltage applications. The liquid electrolyte has a limited operating voltage in the range of 1–5 V,<sup>[58b,74]</sup> which determines the maximum operating voltage of the single cell. In sharp contrast, AECs can withstand even voltages of up to 500–600 V. Therefore, connecting multiple MSCs or SCs in series to achieve high-voltage operation is one way. For example, the Kejten black/CNT-based ultrafast response SCs were connected in series. As shown in Figure 12,<sup>[61,64]</sup> the specific volume capacitance was higher than that of the purchased AECs in a voltage range less than 50 V.

Notably, for an AEC, increasing the thickness of the Al<sub>2</sub>O<sub>3</sub> film (within the range of several micrometers) by chemical aging can easily achieve high voltage resistance. This is a simple strategy without increasing the number of AECs or increasing the size of individual AECs. On the contrary, stacking multiple SCs together is apparently an awkward design that requires complicated control on the uniformity of different cells. Obviously, a single high-voltage ultrafast SC or excellent integration process will be a focus for practical applications. One should consider the trade-off effect between the specific

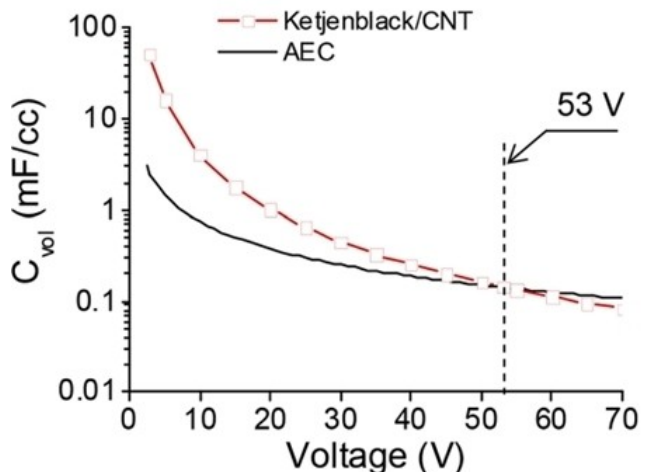


Figure 12. The volumetric capacitance variation as a function of the voltages of a KB SC and an AEC. Reproduced with permission from Ref. [64]. Copyright (2017) Elsevier.

volume capacitance and the absolute size of the cell. Therefore, it is recommended that only low-voltage (< 50–100 V) applications may be suitable for ultrafast response SCs in the future. Considering the technology limits, it is unable to imagine that AECs up to 500–600 V can be replaced by SCs yet.

### 5.5. Management of leakage current

AECs and SCs are both devices with an extralong cycling life exceeding 15 years. Therefore, the quality control of two devices is crucial for long-term usage. AECs consist of  $\text{Al}_2\text{O}_3$ , Al, and organic solvents. Because of their dielectric properties, impurities such as  $\text{Cl}^-$ ,  $\text{F}^-$ ,  $\text{Cu}^{2+}$ , or other ions always exhibit an electrochemical attack on Al. Such behavior of current leakage will weaken the long-life performance of AECs. In worse cases, AECs may be completely destroyed and unable to recover. In addition, explosion occasionally even occurs upon overcharge.

As a comparison, SCs can endure overcharging safely. The leakage current of SCs always means the necessary small current applied to maintain the working state. Meanwhile, the self-discharge of SCs refers to the energy loss when the connection between SCs and the external power is cut. For the self-discharge of SCs, influencing factors include impurities (such as the functional groups of electrodes and  $\text{Cl}^-$ , metal impurities in the electrode and electrolyte), ion mobility of the electrolyte, the pore structure of the electrode, and properties of the membrane.<sup>[75]</sup>

In conclusion, the leakage current concept is different for AECs and SCs. Clearly, it is vital to manage the leakage current of ultrafast response SCs for AC line filtering.

## 6. Conclusion

This review summarizes the progress of ultrafast SCs for the purpose of replacing AECs in AC line filtering. In a short time, many SC systems were reported to exhibit excellent response times and accurate phase angle control. And the system can be optimized by configuration design and the choice of electrolyte, electrode and even the coupled electrode-current collector structure. These achievements deepen the understanding of the structure-performance relationships of SCs and widen the application fields of SCs. Considering the multifactor-influenced application, this review also summarizes the five most important properties for AC filtering. Furthermore, this review provides a relatively long discussion in an attempt to provide sufficient information from the perspective of application demands. Apparently, it would be a great help for scientists and engineering for future R&D in this promising field.

## Acknowledgements

This work is financially supported by NSFC program (No. 22109085 and No. 21975142).

## Conflict of Interest

The authors declare no conflict of interest.

**Keywords:** AC filtering • aluminum electrolyte capacitor • electrolyte • frequency response • supercapacitors

- [1] a) Z. Zhang, M. Liu, X. Tian, P. Xu, C. Fu, S. Wang, Y. Liu, *Nano Energy* **2018**, *50*, 182–191; b) Z.-S. Wu, Z. Liu, K. Parvez, X. Feng, K. Müllen, *Adv. Mater.* **2015**, *27*, 3669–3675; c) J. Joseph, A. Paravannoor, S. V. Nair, Z. J. Han, K. Ostrikov, A. Balakrishnan, *J. Mater. Chem. A* **2015**, *3*, 14105–14108.
- [2] a) J. R. O. Miller, B. C. Holloway, *Science* **2010**, *329*, 1637–1639; b) G. S. Gund, J. H. Park, R. Harpalsinh, M. Kota, J. H. Shin, T.-i. Kim, Y. Gogotsi, H. S. Park, *Joule* **2019**, *3*, 164–176; c) P. S. John R. Miller, *Science* **2008**, *321*, 651–652; d) Z. J. Han, C. Huang, S. S. Meysami, D. Piche, D. H. Seo, S. Pineda, A. T. Murdoch, P. S. Bruce, P. S. Grant, N. Grobert, *Carbon* **2018**, *126*, 305–312; e) Y. Yoo, S. Kim, B. Kim, W. Kim, *J. Mater. Chem. A* **2015**, *3*, 11801–11806.
- [3] a) C. Du, N. Pan, *Nanotechnology* **2006**, *17*, 5314–5318; b) Y. Honda, T. Haramoto, M. Takeshige, H. Shiozaki, T. Kitamura, M. Ishikawa, *Electrochim. Solid-State Lett.* **2007**, *10*, A106.
- [4] Z. Yang, J. Tian, Z. Ye, Y. Jin, C. Cui, Q. Xie, J. Wang, G. Zhang, Z. Dong, Y. Miao, X. Yu, W. Qian, F. Wei, *Energy Storage Mater.* **2020**, *33*, 18–25.
- [5] J. N. Lekitima, K. I. Ozoemena, C. J. Jafta, N. Kobayashi, Y. Song, D. Tong, S. Chen, M. Oyama, *J. Mater. Chem. A* **2013**, *1*, 2821–2826.
- [6] X. Liu, J. Zhu, Y. Li, T. Yang, X. Hao, W. Gong, *Chem. Eng. J.* **2022**, *446*, 136729.
- [7] D. Pech, M. Brunet, H. Durou, P. Huang, V. Mochalin, Y. Gogotsi, P. L. Taberna, P. Simon, *Nat. Nanotechnol.* **2010**, *5*, 651–654.
- [8] F. Han, O. Qian, G. Meng, D. Lin, G. Chen, S. Zhang, Q. Pan, X. Zhang, X. Zhu, B. Wei, *Science* **2022**, *377*, 1004–1007.
- [9] a) J. Lin, C. Zhang, Z. Yan, Y. Zhu, Z. Peng, R. H. Hauge, D. Natelson, J. M. Tour, *Nano Lett.* **2013**, *13*, 72–78; b) Y. J. Kang, Y. Yoo, W. Kim, *ACS Appl. Mater. Interfaces* **2016**, *8*, 13909–13917; c) Z. Wu, L. Li, Z. Lin, B. Song, Z. Li, K. S. Moon, C. P. Wong, S. L. Bai, *Sci. Rep.* **2015**, *5*, 10983; d) D. Zhao, W. Chang, C. Lu, C. Yang, K. Jiang, X. Chang, H. Lin, F. Zhang, S. Han, Z. Hou, X. Zhuang, *Small* **2019**, *15*, e1901494.

- [10] J. R. Miller, R. A. Outlaw, B. C. Holloway, *Electrochim. Acta* **2011**, *56*, 10443–10449.
- [11] R. Burt, G. Birkett, X. S. Zhao, *Phys. Chem. Chem. Phys.* **2014**, *16*, 6519–6538.
- [12] K. V. G. Raghavendra, R. Vinoth, K. Zeb, C. V. V. Muralee Gopi, S. Sambasivam, M. R. Kummarai, I. M. Obaidat, H. J. Kim, *J. Energy Storage* **2020**, *31*, 101652.
- [13] a) E. Frackowiak, F. Béguin, *Carbon* **2001**, *39*, 937–950; b) L. L. Zhang, X. S. Zhao, *Chem. Soc. Rev.* **2009**, *38*, 2520–2531; c) Y. Zhai, Y. Dou, D. Zhao, P. F. Fulvio, R. T. Mayes, S. Dai, *Adv. Mater.* **2011**, *23*, 4828–4850; d) A. G. Pandolfi, A. F. Hollenkamp, *J. Power Sources* **2006**, *157*, 11–27.
- [14] a) J. P. Schmidt, T. Chrobak, M. Ender, J. Illig, D. Klotz, E. Ivers-Tiffée, *J. Power Sources* **2011**, *196*, 5342–5348; b) W. Wu, Y. Zhuang, D. Yan, J. Huang, S. Peng, J. Wang, R. Zhuo, Z. Wu, P. Yan, G. Cao, *J. Power Sources* **2020**, *474*.
- [15] C. Yang, C.-Y. Vanessa Li, F. Li, K.-Y. Chan, *J. Electrochem. Soc.* **2013**, *160*, H271–H278.
- [16] J. F. Robinson, Y. P. Kayinamura, *Chem. Soc. Rev.* **2009**, *38*, 3339–3347.
- [17] A. Allison, H. A. Andreas, *J. Power Sources* **2019**, *426*, 93–96.
- [18] A. Jossen, *J. Power Sources* **2006**, *154*, 530–538.
- [19] R. Kötz, M. Hahn, R. Gallay, *J. Power Sources* **2006**, *154*, 550–555.
- [20] a) X. Chen, R. Paul, L. Dai, *Natl. Sci. Rev.* **2017**, *4*, 453–489; b) K. Sheng, Y. Sun, C. Li, W. Yuan, G. Shi, *Sci. Rep.* **2012**, *2*, 247.
- [21] E. Lust, A. Jänes, M. Arulepp, *J. Electroanal. Chem.* **2004**, *562*, 33–42.
- [22] E. Barsoukov, R. J. Macdonald, *Impedance Spectroscopy: Theory, Experiment, and Applications*, **2005**.
- [23] T. Liu, Z. Zhou, Y. Guo, D. Guo, G. Liu, *Nat. Commun.* **2019**, *10*, 675.
- [24] B. E. Conway, in *Electrochemical Supercapacitors: Scientific Fundamentals and Technological Applications* (Ed.: B. E. Conway), Springer US, Boston, MA, **1999**, pp. 377–416.
- [25] a) P. L. Taberna, P. Simon, J. F. Fauvarque, *J. Electrochem. Soc.* **2003**, *150*, A292–A300; b) Y. Gogotsi, P. Simon, *Science* **2011**, *334*, 917–918; c) P. L. Taberna, P. Simon, J. F. Fauvarque, *J. Electrochem. Soc.* **2003**, *150*, A292; d) G. Ren, X. Pan, S. Bayne, Z. Fan, *Carbon* **2014**, *71*, 94–101; e) X. Yang, J. Zhu, L. Qiu, D. Li, *Adv. Mater.* **2011**, *23*, 2833–2838.
- [26] S. Zhang, Z. Yang, C. Cui, X. Chen, Y. Yu, W. Qian, Y. Jin, *ACS Appl. Mater. Interfaces* **2021**, *13*, 53904–53914.
- [27] K. Sheng, Y. Sun, C. Li, W. Yuan, G. Shi, *Sci. Rep.* **2012**, *2*.
- [28] R. Shao, J. Niu, J. Liang, M. Liu, Z. Zhang, M. Dou, Y. Huang, F. Wang, *ACS Appl. Mater. Interfaces* **2017**, *9*, 42797–42805.
- [29] Y. Zhao, C. Dong, L. Sheng, Z. Xiao, L. Jiang, X. Li, M. Jiang, J. Shi, *ACS Sustainable Chem. Eng.* **2020**, *8*, 8664–8674.
- [30] Y. Rangom, X. Tang, L. F. Nazar, *ACS Nano* **2015**, *9*, 7248–7255.
- [31] L. Pilon, H. Wang, A. d'Entremont, *J. Electrochem. Soc.* **2015**, *162*, A5158–A5178.
- [32] D. R. Rolison, J. W. Long, J. C. Lytle, A. E. Fischer, C. P. Rhodes, T. M. McEvoy, M. E. Bourg, A. M. Lubers, *Chem. Soc. Rev.* **2009**, *38*, 226–252.
- [33] Y. Yoo, M.-S. Kim, J.-K. Kim, Y. S. Kim, W. Kim, *J. Mater. Chem. A* **2016**, *4*, 5062–5068.
- [34] a) J. L. Qi, J. H. Lin, X. Wang, J. L. Guo, L. F. Xue, J. C. Feng, W.-D. Fei, *Nano Energy* **2016**, *26*, 657–667; b) D. Premathilake, R. A. Outlaw, S. G. Parler, S. M. Butler, J. R. Miller, *Carbon* **2017**, *111*, 231–237; c) M. Cai, R. A. Outlaw, R. A. Quinlan, D. Premathilake, S. M. Butler, J. R. Miller, *ACS Nano* **2014**, *8*, 5873–5882; d) M. Cai, R. A. Outlaw, S. M. Butler, J. R. Miller, *Carbon* **2012**, *50*, 5481–5488; e) Z. Wu, L. Li, Z. Lin, B. Song, Z. Li, K.-S. Moon, C.-P. Wong, S.-L. Bai, *Sci. Rep.* **2015**, *5*, 10983; f) C. Zhang, H. Du, K. Ma, Z. Yuan, *Adv. Energy Mater.* **2020**, *10*, 1–17.
- [35] a) M. Cai, R. A. Outlaw, R. A. Quinlan, D. Premathilake, S. M. Butler, J. R. Miller, *ACS Nano* **2014**, *8*, 5873–5882; b) H. Gao, J. Li, J. R. Miller, R. A. Outlaw, S. Butler, K. Lian, *Energy Storage Mater.* **2016**, *4*, 66–70.
- [36] W. Li, S. Azam, G. Dai, Z. Fan, *Energy Storage Mater.* **2020**, *32*, 30–36.
- [37] L. Wang, Z. Li, M. Song, C. Xu, Z. Liu, S. Jia, X. Li, J. Liu, L. Meng, Z. Wang, X. Wang, *Electrochim. Acta* **2021**, *368*, 137561.
- [38] a) N. Islam, J. Warzywoda, Z. Fan, *Nano-Micro Lett.* **2018**, *10*, 9; b) Z. S. Wu, K. Parvez, X. Feng, K. Mullen, *Nat. Commun.* **2013**, *4*, 2487.
- [39] V. K. Mariappan, K. Krishnamoorthy, S. Manoharan, P. Pazhamalai, S. J. Kim, *Small* **2021**, *17*, e2102971.
- [40] J. Lim, U. N. Maiti, N. Y. Kim, R. Narayan, W. J. Lee, D. S. Choi, Y. Oh, J. M. Lee, G. Y. Lee, S. H. Kang, H. Kim, Y. H. Kim, S. O. Kim, *Nat. Commun.* **2016**, *7*, 10364.
- [41] a) H. Liu, M. Zhang, Z. Song, T. Ma, Z. Huang, A. Wang, S. Shao, *J. Alloys Compd.* **2021**, *881*; b) X. Yu, H. S. Park, *Carbon* **2014**, *77*, 59–65; c) C. Long, D. Qi, T. Wei, J. Yan, L. Jiang, Z. Fan, *Adv. Funct. Mater.* **2014**, *24*, 3953–3961; d) Y. Li, G. Wang, T. Wei, Z. Fan, P. Yan, *Nano Energy* **2016**, *19*, 165–175; e) L.-F. Chen, Z.-H. Huang, H.-W. Liang, H.-L. Gao, S.-H. Yu, *Adv. Funct. Mater.* **2014**, *24*, 5104–5111; f) S. Wang, E. Iyyamperumal, A. Roy, Y. Xue, D. Yu, L. Dai, *Angew. Chem. Int. Ed.* **2011**, *50*, 11756–11760.
- [42] Q. Zhou, M. Zhang, J. Chen, J. D. Hong, G. Shi, *ACS Appl. Mater. Interfaces* **2016**, *8*, 20741–20747.
- [43] N. Kurra, M. K. Hota, H. N. Alshareef, *Nano Energy* **2015**, *13*, 500–508.
- [44] Q. Hu, Y. Chai, X. Zhou, S. Ding, D. Lin, N. Jiang, Y. Huo, Q. Zheng, J. Zhao, G. Qu, *J. Colloid Interface Sci.* **2021**, *600*, 256–263.
- [45] A. De Adhikari, N. Shauloff, Y. Turkulets, I. Shalish, R. Jelinek, *Adv. Electron. Mater.* **2021**, *7*, 2100025–2100033.
- [46] a) M. Zhang, F. Héraly, M. Yi, J. Yuan, *Cell Reports Physical Science* **2021**, *2*; b) Q. Jiang, N. Kurra, K. Maleski, Y. Lei, H. Liang, Y. Zhang, Y. Gogotsi, H. N. Alshareef, *Adv. Energy Mater.* **2019**, *9*, 1901061.
- [47] Z. Jiang, Y. Wang, S. Yuan, L. Shi, N. Wang, J. Xiong, W. Lai, X. Wang, F. Kang, W. Lin, C. P. Wong, C. Yang, *Adv. Funct. Mater.* **2018**.
- [48] a) G. Yuan, Y. Liang, H. Hu, H. Li, Y. Xiao, H. Dong, Y. Liu, M. Zheng, *ACS Appl. Mater. Interfaces* **2019**, *11*, 26946–26955; b) L. Sheng, J. Chang, L. Jiang, Z. Jiang, Z. Liu, T. Wei, Z. Fan, *Adv. Funct. Mater.* **2018**, *28*, 1800597; c) M. Zhang, X. Yu, H. Ma, W. Du, L. Qu, C. Li, G. Shi, *Energy Environ. Sci.* **2018**, *11*, 559–565.
- [49] N. Islam, S. Li, G. Ren, Y. Zu, J. Warzywoda, S. Wang, Z. Fan, *Nano Energy* **2017**, *40*, 107–114.
- [50] a) W. Liu, C. Lu, X. Wang, R. Y. Tay, B. K. Tay, *ACS Nano* **2015**, *9*, 1528–1542; b) W.-W. Liu, Y.-Q. Feng, X.-B. Yan, J.-T. Chen, Q.-J. Xue, *Adv. Funct. Mater.* **2013**, *23*, 4111–4122.
- [51] a) G. Ren, S. Li, Z.-X. Fan, M. N. F. Hoque, Z. Fan, *J. Power Sources* **2016**, *325*, 152–160; b) M. Wu, F. Chi, H. Geng, H. Ma, M. Zhang, T. Gao, C. Li, L. Qu, *Nat. Commun.* **2019**, *10*, 2855.
- [52] Z. Bo, W. Zhu, W. Ma, Z. Wen, X. Shuai, J. Chen, J. Yan, Z. Wang, K. Cen, X. Feng, *Adv. Mater.* **2013**, *25*, 5799–5806.
- [53] a) R. Holm, *Electric contacts* **2000**; b) L. Li, J. E. Morris, *IEEE Transactions on Components, Packaging, and Manufacturing Technology: Part A* **1997**, *20*, 3–8.
- [54] a) S. P. Meryl D. Stoller, Yanwu Zhu, Jinho An, Rodney S. Ruoff, *Nano Lett.* **2008**, *8*, 3498–3502; b) P. Simon, Y. Gogotsi, *Nat. Mater.* **2020**, *19*, 1151–1163.
- [55] a) P. Kosyrev, *J. Power Sources* **2012**, *201*, 347–352; b) T. Nathan-Wallesee, I.-M. Lazar, M. Fabritius, F. J. Tölle, Q. Xia, B. Bruchmann, S. S. Venkataraman, M. G. Schwab, R. Mühlaupt, *Adv. Funct. Mater.* **2014**, *24*, 4706–4716.
- [56] C. Yang, K. S. Schellhammer, F. Ortmann, S. Sun, R. Dong, M. Karakus, Z. Mics, M. Löffler, F. Zhang, X. Zhuang, E. Canovas, G. Cuniberti, M. Bonn, X. Feng, *Angew. Chem. Int. Ed. Engl.* **2017**, *56*, 3920–3924.
- [57] Z. Yang, J. Tian, Z. Yin, C. Cui, W. Qian, F. Wei, *Carbon* **2019**, *141*, 467–480.
- [58] a) J. Park, J. Lee, W. Kim, *ACS Energy Lett.* **2021**, *6*, 769–777; b) M. Galiński, A. Lewandowski, I. Stępiński, *Electrochim. Acta* **2006**, *51*, 5567–5580; c) C. Zhong, Y. Deng, W. Hu, J. Qiao, L. Zhang, J. Zhang, *Chem. Soc. Rev.* **2015**, *44*, 7484–7539.
- [59] a) D. R. MacFarlane, N. Tachikawa, M. Forsyth, J. M. Pringle, P. C. Howlett, G. D. Elliott, J. H. Davis, M. Watanabe, P. Simon, C. A. Angell, *Energy Environ. Sci.* **2014**, *7*, 232–250; b) H. V. T. Nguyen, S. Lee, K. Kwak, K.-K. Lee, *Electrochim. Acta* **2019**, *321*, 134649.
- [60] M. Zhang, Q. Zhou, J. Chen, X. Yu, L. Huang, Y. Li, C. Li, G. Shi, *Energy Environ. Sci.* **2016**, *9*, 2005–2010.
- [61] H. Tang, K. Xia, J. Lu, J. Fu, Z. Zhu, Y. Tian, Y. Wang, M. Liu, J. Chen, Z. Xu, Y. Guo, R. Khatoon, H. Chen, Z. Ye, *Nano Energy* **2021**, *84*, 105931.
- [62] J. Park, W. Kim, *Adv. Energy Mater.* **2021**, *11*, 2003306.
- [63] a) Y. Korenblit, M. Rose, E. Kockrick, L. Borchardt, A. Kvít, S. Kaskel, G. Yushin, *ACS Nano* **2010**, *4*, 1337–1344; b) F. Chi, C. Li, Q. Zhou, M. Zhang, J. Chen, X. Yu, G. Shi, *Adv. Energy Mater.* **2017**, *7*, 1700591–1700599.
- [64] Y. Yoo, J. Park, M.-S. Kim, W. Kim, *J. Power Sources* **2017**, *360*, 383–390.
- [65] D. Pech, M. Brunet, P.-L. Taberna, P. Simon, N. Fabre, F. Mesnilgrente, V. Conédéra, H. Durou, *J. Power Sources* **2010**, *195*, 1266–1269.
- [66] a) Z. S. Wu, Z. Liu, K. Parvez, X. Feng, K. Mullen, *Adv. Mater.* **2015**, *27*, 3669–3675; b) K. Gao, S. Wang, W. Liu, Y. Yue, J. Rao, J. Su, L. Li, Z. Zhang, N. Liu, L. Xiong, Y. Gao, *ChemElectroChem* **2019**, *6*, 1450–1457.
- [67] A. Izadi-Najafabadi, D. N. Futaba, S. Iijima, K. Hata, *J. Am. Chem. Soc.* **2010**, *132*, 18017–18019.
- [68] a) Z. Bo, C. Xu, H. Yang, H. Shi, J. Yan, K. Cen, K. Ostrikov, *ChemElectroChem* **2019**, *6*, 2167–2173; b) F. Chi, Y. Hu, W. He, C. Weng, H. Cheng, C. Li, L. Qu, *Small* **2022**, *18*, 2200916.
- [69] a) G. Feng, M. Chen, S. Bi, Z. A. H. Goodwin, E. B. Postnikov, N. Brilliantov, M. Urbakh, A. A. Kornyshev, *Phys. Rev. X* **2019**, *9*, 021024; b) Z. Z. Yunda Wang, T. Usui, M. Benedict, S. Hirose, J. Lee, J. Kalb, D.

- Schwartz, *Nat. Mater.* **2020**, *370*, 129–133; c) D.-D. Li, Y.-R. Yang, X.-D. Wang, G. Feng, *J. Phys. Chem. C* **2020**, *124*, 15723–15729.
- [70] T. Jin, X. Ji, P.-F. Wang, K. Zhu, J. Zhang, L. Cao, L. Chen, C. Cui, T. Deng, S. Liu, N. Piao, Y. Liu, C. Shen, K. Xie, L. Jiao, C. Wang, *Angew. Chem. Int. Ed.* **2021**, *60*, 11943–11948.
- [71] a) W. Liu, C. X. Lu, X. L. Wang, R. Y. Tay, B. K. Tay, *ACS Nano* **2015**, *9*, 1528–1542; b) J. R. Miller, R. A. Outlaw, *J. Electrochem. Soc.* **2015**, *162*, A5077–A5082; c) M. Zhang, W. Wang, L. Tan, M. Eriksson, M. Wu, H. Ma, H. Wang, L. Qu, J. Yuan, *Energy Stor. Mater.* **2021**, *35*, 327–333.
- [72] J. Zhao, Y. Zhang, J. Yan, X. Zhao, J. Xie, X. Luo, J. Peng, J. Wang, L. Meng, Z. Zeng, C. Lu, X. Xu, Y. Dai, Y. Yao, *ACS Appl. Energy Mater.* **2019**, *2*, 993–999.
- [73] L. Wang, L. Zhao, M. Song, L. Xie, X. Wang, X. Li, Y. Huang, M. Wei, Q. Jin, X. Meng, Y. Zhao, *J. Energy Chem.* **2022**.
- [74] L. Wei, W. Jiang, Y. Yuan, K. Goh, D. Yu, L. Wang, Y. Chen, *J. Solid State Chem.* **2015**, *224*, 45–51.
- [75] K. Liu, C. Yu, W. Guo, L. Ni, J. Yu, Y. Xie, Z. Wang, Y. Ren, J. Qiu, *J. Energy Chem.* **2021**, *58*, 94–109.

Manuscript received: January 5, 2023

Revised manuscript received: January 31, 2023

Version of record online: February 17, 2023